Correlation between structural stability and substrate specificity of DNMT1

(DNMT1 の構造安定性と基質特異性との相関)

A doctoral thesis

By

Kensaku Kanada

Submitted to the Graduate School of Science

Osaka University

Japan

May, 2017

Acknowledgement

I would like to express the deepest appreciation to Professor Atsushi Nakagawa (Laboratory of Supramolecular Crystallography, Institute for Protein Research, Osaka University) and Professor Shoji Tajima (Laboratory of Epigenetics, Institute for Protein Research, Osaka University) for their management of my research and constantly gracious guidance from an educational standing point of view. I would like to offer my special thanks to Associate Professor Isao Suetake (Laboratory of Epigenetics, Institute for Protein Research, Osaka University) and Specially Appointed Assistant Professor Kohei Takeshita (Laboratory of Supramolecular Crystallography, Institute for Protein Research, Osaka University) for their support for my experiments, insightful comments and warm encouragement. They taught me many techniques, which are Sf9 expression system, biochemistry, crystallization and so on. I would like to thank Professor Genji Kurisu (Laboratory of Protein Crystallography, Institute for Protein Research, Osaka University) and Professor Takahide Kon (Laboratory of Cell Motility, Department of Biological Sciences, Osaka University) for their helpful suggestions and constructive comments for improvement of this doctoral thesis. I also thank all members of the Laboratory of Supramolecular Crystallography and the Laboratory of Epigenetics for their suggestions, comments, and kind support in many aspects. Finally, I thank my family members for their supports.

Table of contents

Abbreviations

5MC	5-methylcytosine
5fC	5-fluorocysotine
ADCA-DN	Autosomal dominant cerebellar ataxia, deafness and narcolepsy
ADD	Alpha thalassaemia/mental retardation syndrome X-linked homologue (ATRX)-DNMT3-DNMT3L
AdoHcy	*S*-adenosyl-L-homocysteine
AdoMet	*S*-adenosyl-L-methionine
BAH	Bromo-adjacent homology
CCP4	Collaborative Computing Project 4
CBB	Coomassie Brilliant Blue
CDKL5	Cyclin-dependent kinase-like 5
CMT3	Chromomethylase 3
CREB	cAMP response element binding protein
CTCF	CCCTC-binding factor
DIM-2	Defective in methylation-2
DMAP1	DNMT1-associated protein 1
DNMT1	DNA methyltransferase 1
DNMT1A	DNA methyltransferase 1A
DNMT3A	DNA methyltransferase 3A
DNMT3B	DNA methyltransferase 3B
DNMT3L	DNA methyltransferase 3-like
GST	Glutathione *S*-transferase
MBD	Methyl-CpG-binding domain
MBD1	Methyl-CpG-binding domain protein 1

MBD2	Methyl-CpG-binding domain protein 2
MBD3	Methyl-CpG-binding domain protein 3
MBD4	Methyl-CpG-binding domain protein 4
MET1	Methyltransferase 1
MET1B	Methyltransferase 1B
MeCP2	Methyl-CpG-binding protein 2
N-CoR	Nuclear receptor co-repressor
NTD	N-terminal independently folded domain
NuRD	Nucleosome remodeling and histone deacetylase
PCNA	Proliferating cell nuclear antigen
PDB	Protein Data Bank
PEG	Polyethylene glycol
PMSF	Phenylmethylsulfonyl fluoride
PWWP	Pro-Trp-Trp-Pro
RFTS	Replication foci-targeting sequence
Rb	Retinoblastoma gene product
SDS-PAGE	Sodium dodecyl sulfate-polyacrylamide gel electrophoresis
SET7	SET domain containing lysine methyltransferase 7
SETDB1	SET domain bifurcated 1
SPring-8	Super Photon ring-8 GeV
SRA	Su(var)3-9, En(zeste), and Trithorax (SET) and really interesting new gene (RING) finger-associated
TCEP-HCl	Tris(2-carboxyethyl)phosphine Hydrochloride
TRD	Target recognition domain
UHRF1	Ubiquitin-like, containing plant homeodomain (PHD) and really interesting new gene (RING) finger domains 1

USP7	Ubiquitin-Specific Protease 7
ZBTB	Zinc finger and BTB

Chapter 1
Introduction

1.1 Epigenetics

A single zygote differentiates into a variety of cells, which have different morphology and function, in spite of possessing the identical genetic information. During this process, the amount and timing of gene expression are regulated to gain cell-specific phenotype. These gene expression patterns are established and maintained mainly by the mechanism of "epigenetics", which is defined as follows: "An epigenetic trait is a stably heritable phenotype resulting from changes in a chromosome without alterations in the DNA sequence" (Berger *et al*., 2009). The epigenetic mechanism is based on covalent bonds of DNA methylation and histone post-transcriptional modifications.

Genome DNA is packed into chromosomes in the nucleus. In eukaryotes, a histone octamer comprising two sets of core histones H2A, H2B, H3 and H4, is wrapped 1.7 times with 147 base pair-DNA to form a nucleosome (Luger *et al*., 1997). Nucleosomes forming "beads on a string" structure are folded into 30 nm chromatin fibers (Margueron and Reinberg, 2010), and these fibers are condensed into a chromosome. The N-terminal tail regions of each histone protrude from a nucleosome are subjected to acetylation, methylation, phosphorylation, ubiquitylation and so on (Kouzarides, 2007). Two different packing states of chromatin exist; highly condensed heterochromatin containing silenced genes, and unraveled euchromatin containing modifications that are involved in active transcription. Combinations of DNA and histone modifications play a role in modulating chromatin conformation (Cheng and Blumenthal, 2010), and control the access of readers and modifiers, and thus differences of these modifications result in variation of gene expression patterns (Ruthenburg *et al*., 2007).

1.2 DNA methylation and gene regulation

In prokaryote, methylation modification is found in the fifth position of the cytosine bases (C5), the sixth position of adenine bases (N6), and the fourth position of cytosine (C4) (Kumar *et al*., 1994). The C5 methylation plays a role in "restriction-modification systems" that protects DNA from digestion by restriction enzymes and bacteriophage infection (Wilson and Murray, 1991). In eukaryote, recently adenine methylation has been found in *clamidomonas*, *drosophila*, and *C. elegance* (Fu *et al.*, 2015; Zhang *et al*., 2015; Greer *et al*., 2015). However, methylation at the fifth position of cytosine base is the major modification in eukaryotes. The 5-methylcytosine was first discovered in calf thymus DNA (Hotchkiss, 1948). Two papers independently proposed that 5-methylcytosines are inherited during cell divisions, and predicted the existence of two kinds of enzymes to methylate the un-methylated DNA and the methylated DNA on one strand, which is so-called "hemi-methylated DNA" (Holliday and Pugh, 1975; Riggs, 1975). In addition, they postulated that 5-methylcytosine contributes to gene silencing. Thereafter, these postulations have been confirmed in the 1980s. The 5-methylcytosine in genome DNA plays an important role in development and differentiation (Reik, 2007), transcriptional silencing of retrotransposons (Walsh *et al*., 1998; Bourc'his and Bestor, 2004), X-chromosome inactivation in females (Reik and Lewis, 2005), and genomic imprinting (Li *et al*., 1993).

DNA methylation in mammals occurs selectively at the cytosine of CpG sequences (Figure 1.1). DNA methylation at non-CpG sequences, which occurs at the cytosine of CpT and CpA sequences, is observed in embryonic stem cells (Ramsahoye *et al*., 2000; Lister *et al*., 2009), but this methylation pattern is not maintained by maintenance DNA methyltransferase DNMT1 during replication. As expected, non-proliferating cell containing tissues such as ovary (Shirane *et al*., 2013) and brain (Guo *et al*., 2014) contain relatively high level of non-CpG methylation. In plant, in addition to CpG, CpHpG and

CpHpH sequences (in which H = A, T, or C) are also methylated and maintained (Law and Jacobsen, 2010).

About 70 to 80% of CpG sequences in human somatic tissues are methylated (Ehrlich *et al*., 1982). The CpG sequences in satellite DNAs, repetitive elements, non-repetitive intergenic DNA, and exons of genes (Li and Zhang, 2014) are generally highly methylated. Approximately 70% of gene promoters in vertebrates contain CpG-enriched sequences of more than 1,000 base pairs, which are called CpG islands, and most of them are at the promoters of housekeeping genes (Deaton and Bird, 2011). In somatic cells, promoter CpG islands of housekeeping genes are under methylated, and these CpG islands contribute to transcriptionally permissive chromatin environment (Long *et al*., 2013). DNA methylation of CpG islands at gene promoters leads to transcriptionally inactive (Deaton and Bird, 2011). Unlike CpG islands in promoter regions, most gene bodies are CpG-poor state in vertebrates, and the CpG sites are frequently methylated (Jones, 2012). As gene-body methylation level of exons is observed to be higher than that of introns and transitions of methylation level occur at boundaries between exon and intron, it was proposed that gene body methylation may contribute to transcript splicing (Laurent et al., 2010).

DNA methylation plays a role in regulation of gene expression through two pathways: The methylated target sites in promoters or insulators interfere with the binding of transcription factors, or the co-repressor complex containing methyl-CpG binding proteins that selectively bind to methylated DNA establishes silent chromatin. As for the first mechanism, most of the transcription factors are inhibited the binding to the methylated CpG in the binding motif or adjacent sequence. Although it is shown that the transcription factors such as CCCTC-binding factor (CTCF) (Bell *et al*., 1999), E2F (Campanero *et al*., 2000), or CREB (Iguchi-Ariga and Schaffner, 1989) are inhibited by the methylation of the binding motifs and near, it does not mean that the mechanism is

working *in vivo*. The methylation of the binding motif of CTCF in the Igf2 and H19 imprinting locus is the only example that is shown to contribute to the *in vivo* regulation (Bell and Felsenfeld, 2000; Hark *et al*., 2000).

As for the second mechanism, three classes of mammalian methyl-CpG binding proteins are identified (Hashimoto *et al*., 2015). MeCP2, MBD1, MBD2, MBD3 and MBD4 belong to the methyl-CpG-binding domain (MBD) family. MeCP2, MBD1, MBD2, and MBD4 selectively bind to the methylated DNA, and these proteins contribute in silencing transcription (Bogdanović and Veenstra, 2009). MeCP2 interacts with Sin3A co-repressor complex containing histone deacetylase (Nan *et al*., 1998). *Mecp2* is located on X-chromosome, and its mutation causes Rett syndrome, which is an X-linked neuro-developmental disorder (Amir *et al*., 1999). MBD1 associates with SET domain bifurcated 1 (SETDB1) and was reported to contribute to maintenance of histone H3 lysine 9 methylation during DNA replication (Sarraf and Stancheva, 2004). The histone H3 K9 methylation is involved in chromatin silencing. MBD1 also binds to un-methylated CpG through a CXXC motif, which has similar sequences to that of DNMT1 (Jørgensen *et al*., 2004). MBD2 forms the complex with nucleosome remodeling and histone deacetylase (NuRD) co-repressor (Feng and Zhang, 2001).

The second class is Ubiquitin-like, containing plant homeodomain (PHD) and really interesting new gene (RING) finger domains 1 (UHRF1). UHRF1 binds to hemi-methylated DNA through Su(var)3-9, En(zeste), and Trithorax (SET) and RING finger-associated (SRA) domain (Arita *et al.*, 2008; Avvakumov *et al.*, 2008; Hashimoto *et al.*, 2008).

The third class is the Cys2His2 (C2H2) Zinc finger protein family, which contains Kaiso, ZBTB4, and ZBTB38. Kaiso binds to nuclear receptor co-repressor (N-CoR) deacetylase complex (Yoon *et al.*, 2003). ZBTB4 and ZBTB38 show distinct tissue-specific expression pattern, and are highly expressed in the brain (Filion *et al*., 2006).

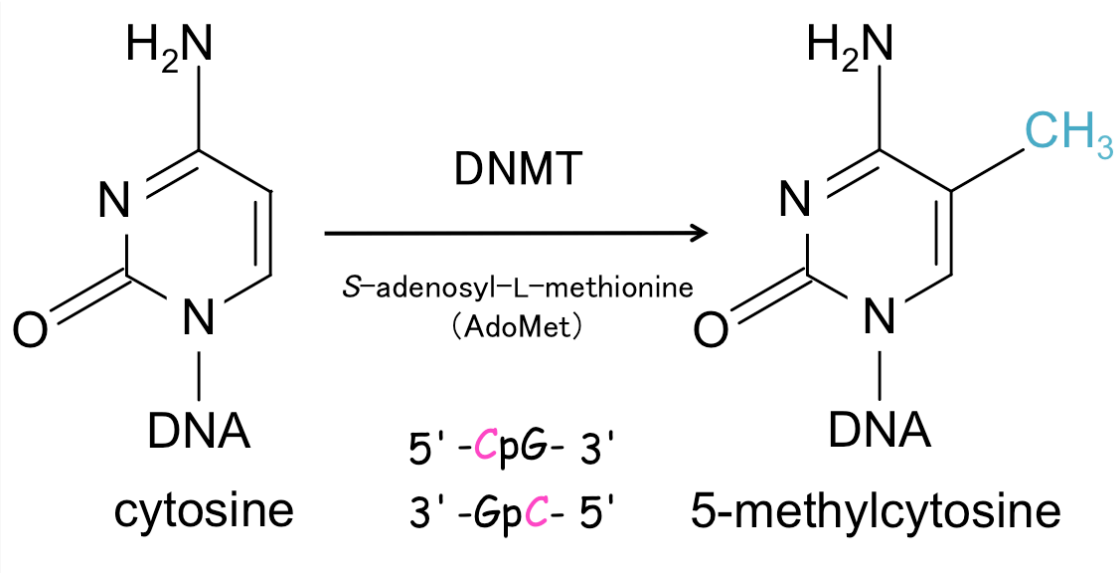

Figure 1.1 DNA methylation at cytosine base.

In mammals, DNMT methylates the fifth of cytosine in CpG sequences by transfer of a methyl group from *S*-adenosyl-L-methionine (AdoMet) to the cytosine.

1.3 Mammalian DNA (cytosine-C5) methyltransferases

Mammals possess the three active DNA (cytosine-C5) methyltransferase, which are DNMT1, DNMT3A, and DNMT3B (Figure 1.2). DNMT1 has the higher methylation activity toward hemi-methylated CpG than un-methylated CpG (Vilkaitis *et al*., 2005). DNMT3A and DNMT3B equally methylate dIdC and dCdG *in vivo*, and are also subtly able to methylate the cytosine of CpT and CpA sequences (Suetake *et al*., 2003). These DNMT3s are responsible for *de novo*-type DNA methylation activity, and thus are responsible in establishing DNA methylation patterns during embryogenesis and gametogenesis (Okano *et al*., 1999; Kaneda *et al*., 2004). In addition, DNMT3 like protein (DNMT3L), which is a catalytically inactive homolog of the DNMT3 family, is prerequisite for the *de novo* methylation in germ cells as a regulatory factor of DNMT3A (Jia *et al*., 2007). DNMT3L directly interacts with DNMT3A or DNMT3B through their C-terminal domains, and these interactions stimulate each DNA methylation activity *in vitro* (Suetake *et al*., 2004). There are two waves of the establishment of DNA methylation patterns in mammalian life cycle (Rose and Klose, 2014). The first wave of *de novo* methylation starts to occur in the inner cell mass cells at around the time of implantation by DNMT3B (Watanabe *et al*., 2002). Next, DNA methylation patterns in primordial germ cell are re-established by DNMT3A2, a short isoform of DNMT3A, and DNMT3L during germ line development (Sakai *et al*., 2004). Once genome DNA methylation patterns are established, DNMT1 inherits these patterns by methylation of hemi-methylated CpG during cell divisions.

All mammalian DNMTs consist of the N-terminal regulatory region and the C-terminal catalytic domain. The C-terminal catalytic domains of mammalian DNMTs share the ten conserved motifs among DNA (cytosine-C5) methyltransferases from prokaryote to eukaryote. In particular, motifs I, IV, VI, VIII, IX, and X are highly conserved in all DNA (cytosine-C5) methyltransferases. The nonconserved region

between motifs VIII and IX contains the target recognition domain (TRD), which is involved in recognition of DNA substrate sequence. The TRD of DNMT1 is larger than that of DNMT3s, and plays a role in recognizing hemi-methylated CpG. DNA (cytosine-C5) methyltransferases catalyze the transfer of a methyl group from *S*-adenosyl-L-methionine as the supplier of the methyl group to the fifth position of the flipped out target cytosine of DNA double helix. This transfer mechanism had been researched on prokaryotic DNA (cytosine-C5) methyltransferases (Figure 1.3) (Wu and Santi, 1987) and mammalian DNMTs adopt the similar mechanism (Yang *et al*., 2013). The initial step of this transfer mechanism is the nucleophilic attack on the sixth carbon of a target cytosine by the completely conversed cysteine thiol of prolyl-cysteinyl dipeptide in motif IV, and a covalent DNA-enzyme intermediate is generated. This attack leads to the transfer of the methyl group in *S*-adenosyl-L-methionine to the fifth carbon of the target cytosine. Finally, the fifth proton is abstracted, and the covalent bond between the cysteine thiol and the sixth carbon of the target cytosine is eliminated by a β-elimination.

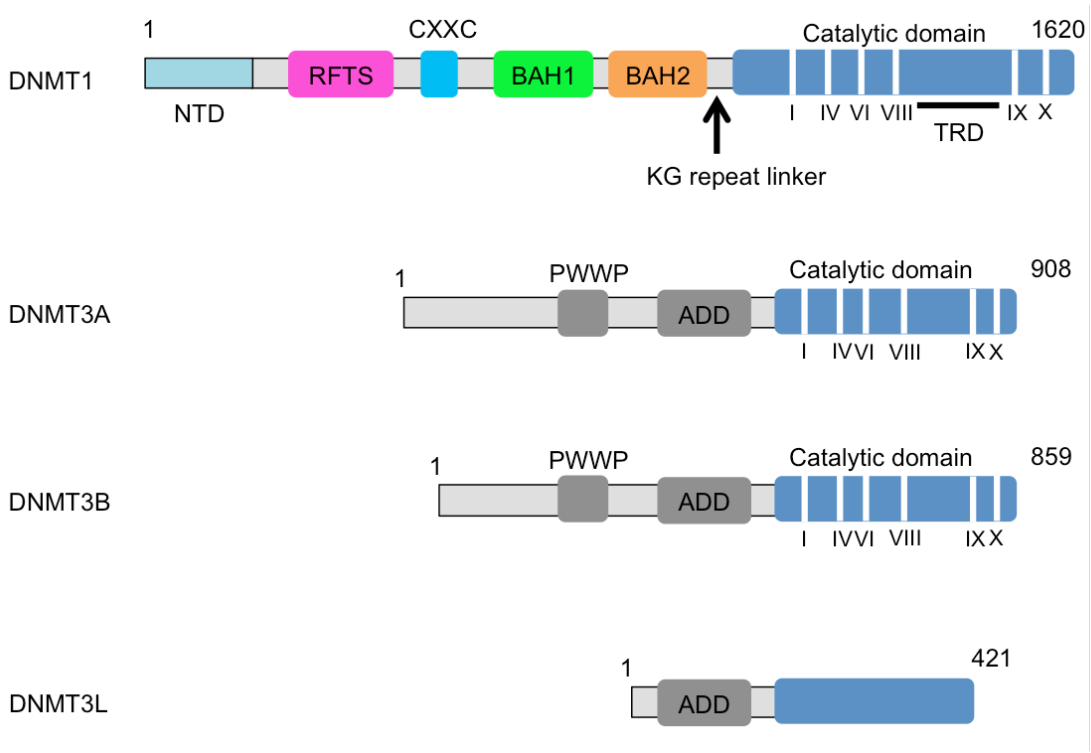

Figure 1.2 Schematic illustrations of mouse DNA (cytocin-5) methyltransferases.

DNMT1 has the N-terminal independently folded domain (NTD), the replication foci-targeting sequence (RFTS) domain, the zinc-finger-like (CXXC) motif, two tandem bromo-adjacent homology (BAH) domains BAH1 and BAH2, the KG repeat liner and the catalytic domain. The catalytic domain contains the target recognition domain (TRD) and conserved motifs (I–X). DNMT3A and DNMT3B have the Pro-Trp-Trp-Pro (PWWP) domain, the alpha thalassaemia/mental retardation syndrome X-linked homologue (ATRX)-DNMT3-DNMT3L (ADD) domain, and the C-terminal catalytic domain. DNMT3L does not have any conserved motifs in the catalytic domain.

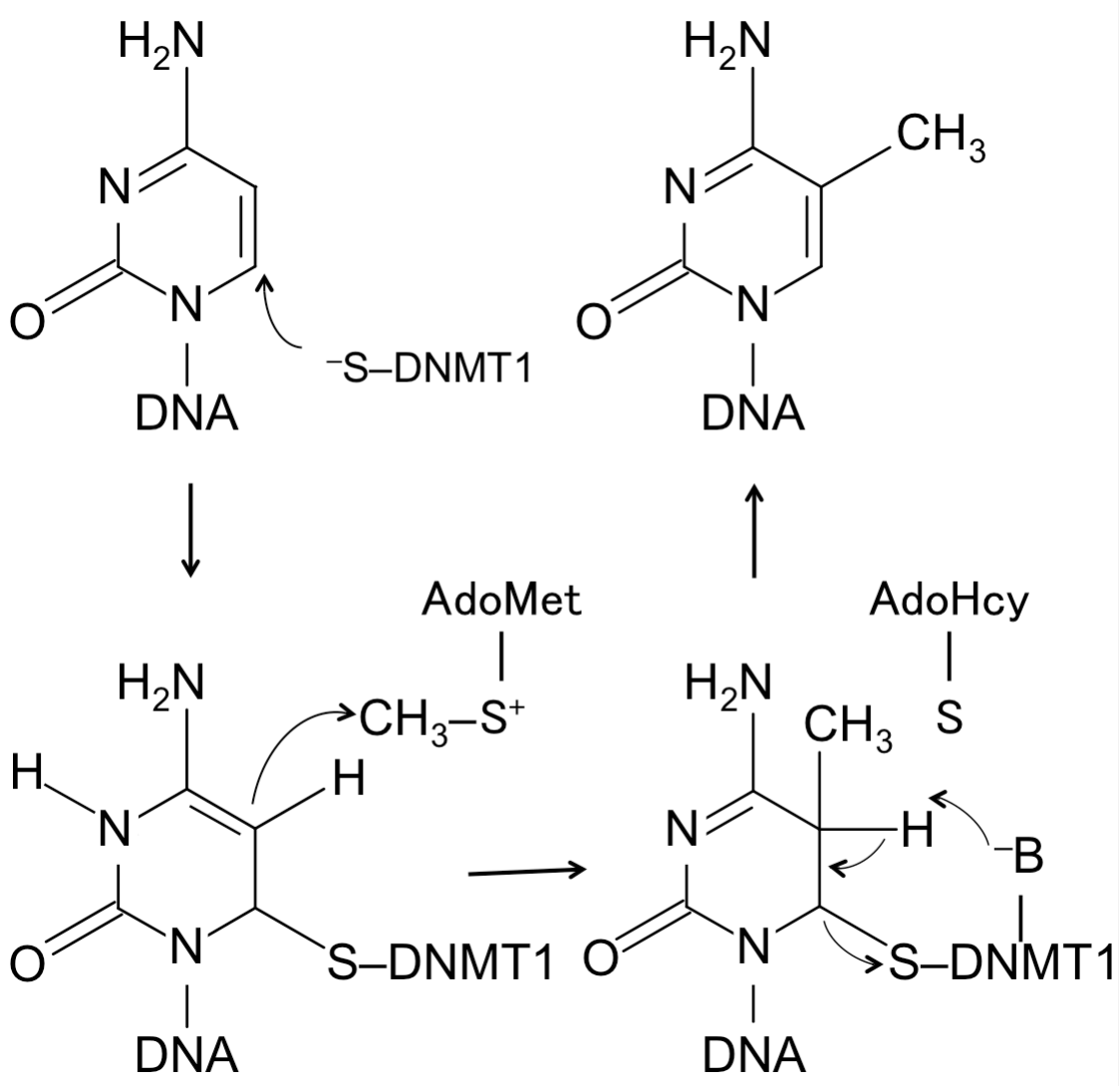

Figure 1.3 The mechanism of cytosine methylation.

1.4 *De novo* DNA methylation by DNMT3 family

DNMT3A and DNMT3B have common domain arrangements (Figure 1.2). Both DNMT3s comprise the Pro-Trp-Trp-Pro (PWWP) domain, the alpha thalassaemia/mental retardation syndrome X-linked homologue (ATRX)-DNMT3-DNMT3L (ADD) domain, and the C-terminal catalytic domain. The PWWP domain of DNMT3A or DNMT3B binds to tri-methylated lysine 36 residues of histone H3 tails (H3K36me3) (Rondelet *et al*., 2016), and the PWWP domain of DNMT3B contributes to targeting of DNMT3B to gene body methylation (Morselli *et al*., 2015). The C-terminal domains of DNMT3A and DNMT3L form a dimer, and then this dimer forms a tetramer with a DNMT3A–DNMT3A interface and two DNMT3A–DNMT3L interfaces in the crystal structure (Jia *et al*., 2007). Recently, the crystal structure of the tetramer of DNMT3A harboring the ADD domain and DNMT3L in complex with or without histone H3 tail was reported (Guo *et al*., 2015). The tetramer without histone H3 tail shows that the ADD domain interacts with the catalytic domain of DNMT3A and it inhibits DNA methylation activity of the tetramer. On the other hand, the tetramer in complex with histone H3 tail shows that the binding of histone H3 tail to the ADD domain disrupts the interaction between the ADD domain and the catalytic domain of DNMT3A, and DNA methylation activity of the tetramer increases. In addition, tri-methylated lysine 4 residues of histone H3 tails (H3K4me3) do not bind to the ADD domain (Otani *et al*., 2009). These observations explain the molecular mechanism of the negative correlation between DNA methylation and H3K4me3 in mammalian genome.

1.5 Maintenance-type DNA methyltransferase DNMT1

The N-terminal regulatory region of DNMT1 harbors the N-terminal independently folded domain (NTD) (Suetake *et al*., 2006), the replication foci-targeting sequence (RFTS) domain (Leonhardt *et al*., 1992), the zinc-finger-like (CXXC) motif, and two tandem bromo-adjacent homology (BAH) domains. Then, the lysyl-glycyl (KG) repeats linker connects to the C-terminal catalytic domain (Figure 1.2). The NTD is the N-terminal about 250 amino acid sequences, and it binds to the DNMT1-associated protein 1 (DMAP1), which is a transcriptional repressor (Rountree *et al*., 2000), the retinoblastoma gene product (Rb), which is a cell cycle regulator (Pradhan and Kim, 2002), DNMT3A and DNMT3B (Kim *et al*., 2002), the proliferating cell nuclear antigen (PCNA), which is an auxiliary factor in DNA replication (Chuang *et al*., 1997), the cyclin-dependent kinase-like 5 (CDKL5 kinase) (Kameshita *et al*., 2008), the casein kinase 1δ/ε (Sugiyama *et al*., 2010) and so on. Therefore, it has been speculated that the NTD plays a role in a platform for interaction with factors to regulate the function and localization of DNMT1 (Suetake *et al*., 2006).

DNMT1 is highly expressed in early S-phase in cell cycle, and it is decreased during late S-phase. PCNA recruits DNMT1 to replication foci, but it is not absolutely essential for replication coupled DNA methylation (Garvilles *et al*., 2015). On the other hand, UHRF1 is essential for maintenance DNA methylation by DNMT1 *in vivo*, and it co-localizes with DNMT1 at replication foci during S-phase (Bostick, *et al*., 2007; Sharif *et al*., 2007). The RING finger domain of UHRF1 possesses E3 ubiquitin ligase activity. This domain ubiquitinates lysine 18 (Qin *et al*., 2015) and lysine 23 (Nishiyama *et al*., 2013) residues of histone H3 tails (H3K18 and K23ubq), and these modifications interact with the RFTS domain and contribute to maintenance DNA methylation *in vivo*.

The stability and abundance of DNMT1 are modulated by post-translational modifications such as methylation, phosphorylation, acetylation and ubiquitination (Qin

et al., 2011; Kar *et al*., 2012). Phosphorylation of S143 in human DNMT1 by AKT1 kinase stabilizes the DNMT1 during mid-S-phase. The crystal structure of human DNMT1 complex with SET7 suggests that phosphorylated S143 blocks methylation of the adjacent K142 by SET7, which is a mark to degrade DNMT1 (Estève *et al*., 2011). Recently, the crystal structure of human DNMT1 complex with ubiquitin-like domains of the Ubiquitin-Specific Protease 7 (USP7) was reported, suggesting that the interaction between ubiquitin-like domains of USP7 and the KG repeat linker of DNMT1 prevents acetylation of lysines in the KG repeat linker, which leads to ubiquitination and degradation of DNMT1, and promotes deubiquitination of DNMT1 (Cheng *et al*., 2015).

1.6 Structural basis for maintenance DNA methylation by DNMT1

Maintenance DNA methylation is the process that genome DNA methylation patterns are faithfully inherited to next generation. In this process, DNMT1 is responsible for methylating the nascent strand CpG of the hemi-methylated CpG that emerges just after DNA replication (Figure 1.4) (Goll and Bestor, 2005). DNA methylation patterns of some regions are maintained with 99.9% fidelity per cell division *in vivo* (Ushijima *et al*., 2003). However, the fidelity of maintenance DNA methylation by DNMT1 *in vitro* is about 95% (Vilkaitis *et al*., 2005). This difference probably results from the regulations by modifications to DNMT1, the interaction between some factors and the NTD of DNMT1, and the support by UHRF1, which acts as an essential factor for maintenance DNA methylation.

Our group determined the crystal structure of mouse DNMT1, which comprises 291–1620 amino acid residues (DNMT1(291–1620)) (Figure 1.5) (Takeshita *et al*., 2011; PDB accession number: 3AV4). The RFTS domain occludes in the DNA binding pocket of the catalytic domain, and the hydrogen bonds between these domains fix the position of the RFTS domain. Therefore, the plugged RFTS domain should be removed from the DNA binding pocket to bind the substrate DNA (Takeshita *et al*., 2011; Syeda *et al*., 2011; Berkyurek *et al*., 2014). In fact, the difference of the activation energy between wild type DNMT1(291–1620) and DNMT1(602–1620) lacking the RFTS domain on maintenance DNA methylation activity is about 80 kJ/mol, and several DNMT1(291–1620) mutations that are impaired these hydrogen bonds lowered the activation energy (Takeshita *et al*., 2011; Berkyurek *et al*., 2014). The RFTS domain of DNMT1 is mainly responsible for the replication coupled DNA methylation since DNMT1 lacking the RFTS domain is not localized to replication foci and partially does not maintain DNA methylation *in vivo* (Garvilles *et al*., 2015). In addition, the full-length DNMT1 and DNMT1(291–1620) show equivalent maintenance methylation activity in a processive manner, and therefore

the NTD is not necessary for maintenance DNA methylation activity *in vitro* (Vilkaitis *et al*., 2005).

The RFTS domain interacts with the SET and RING finger-associated (SRA) domain of UHRF1 and this interaction increases the maintenance DNA methylation activity of DNMT1 comprising the RFTS domain (Berkyurek *et al*., 2014). The SRA domain specifically binds to hemi-methylated CpG and it plays a role in faithful maintenance DNA methylation *in vivo*. These observations indicate that the SRA domain promotes to release the RFTS domain from the DNA binding pocket (Berkyurek *et al*., 2014) and transfers hemi-methylated DNA to DNMT1 (Arita *et al*., 2008). On the other hand, DNMT1(291–1620) shows the maintenance DNA methylation activity without the SRA domain *in vitro*, and thus the RFTS domain of DNMT1 should be released from the DNA binding pocket by DNMT1 itself or DNA substrates. In addition, some mutations in the RFTS domain surface contacting with the catalytic domain cause the autosomal dominant cerebellar ataxia, deafness and narcolepsy (ADCA-DN) (Winkelmann *et al*., 2012). In these mutations, A554 and V590 in human DNMT1 form a hydrophobic cluster, suggesting that these mutations may lead to local structural perturbation of the RFTS domain surface (Zhang *et al*., 2015).

The crystal structure of mouse DNMT1 comprising residues 650–1602 (DNMT1(650–1602)), which lacks the RFTS domain, in complex with un-methylated DNA shows that the un-methylated DNA binds to the CXXC motif, and a linker between this CXXC motif and the BAH domain, which is called the auto-inhibition linker, is pushed to the DNA binding pocket (Figure 1.5) (Song *et al*., 2011; PDB accession number: 3PT6). This crystal structure suggests that the CXXC motif and the auto-inhibition linker inhibit the accession of un-methylated DNA to the DNA binding pocket, thereby preventing *de novo* DNA methylation of DNMT1. The CXXC motif of this crystal structure is located on a similar position as that of the crystal structure of human

DNMT1 comprising residues 601–1600 without DNA (PDB accession number: 3SWR). However, our DNMT1(291–1620) and DNMT1(602–1620) shows significant *de novo* DNA methylation activity (Takeshita *et al*., 2011). Therefore, the crystal structure of mouse DNMT1(650–1602) in complex with un-methylated DNA may be an artifact structure.

The function of the two BAH domains of DNMT1 are unclear. The *Arabidopsis thaliana* chromomethylase 3 (CMT3) in the plant-specific chromomethylase family, which methylates the cytosine of CpNpG sequences, possesses the BAH domain. The aromatic cage of this domain binds to di-methylated lysine 9 residues of histone H3 tails (H3K9me2) (Du *et al*., 2012). On the other hand, the binding of the two BAH domains in DNMT1 to nucleosome is not observed (Onishi *et al*., 2007), although the N-terminal BAH domain of DNMT1 has an aromatic cage.

The crystal structure of mouse DNMT1 comprising residues 731–1602 (DNMT1(731–1602)), which lacks the RFTS domain and the CXXC motif, in complex with hemi-methylated-mimicking DNA containing 5-fluorocytosine shows that the hemi-methylated DNA binds to DNA binding pocket of the catalytic domain (Figure 1.5) (Song *et al*., 2012; PDB accession number: 4DA4). The TRD in the catalytic domain overhangs along the hemi-methylated DNA, and the target 5-fluorocytosine is flipped out of double stranded DNA helix in the catalytic center, in which the sixth carbon of 5-fluorocytosine forms a covalent bond with the thiol of C1229 of prolyl-cysteinyl dipeptide in motif IV (Figure 1.6A).

This crystal structure of mouse DNMT1(731–1602) in complex with hemi-methylated DNA also shows the interaction manner between the TRD and 5-methylcytosine of hemi-methylated DNA (Figure 1.6B) (Song *et al*., 2012). The side chains of C1501, L1502, W1512, L1515, and M1535 from the TRD loops form a hydrophobic cage harboring the 5-methyl group of the 5-methylcytosine. The mouse

DNMT1 mutants harboring C1501A, L1502A, L1515A, and M1535A show 2- to 4 times reduction in DNA methylation activity toward hemi-methylated DNA and 3- to 4 times reduction in DNA methylation activity toward un-methylated DNA, compared with wild type DNMT1(731–1602) (Song *et al*., 2012). Also, the indole ring of W1512 partially makes a base-stacking interaction with the 5-methylcytosine, and the DNMT1 mutant harboring W1512A or W1512L is almost inactivated in DNA methylation activity, respectively (Takeshita *et al*., 2011; Song *et al*., 2012).

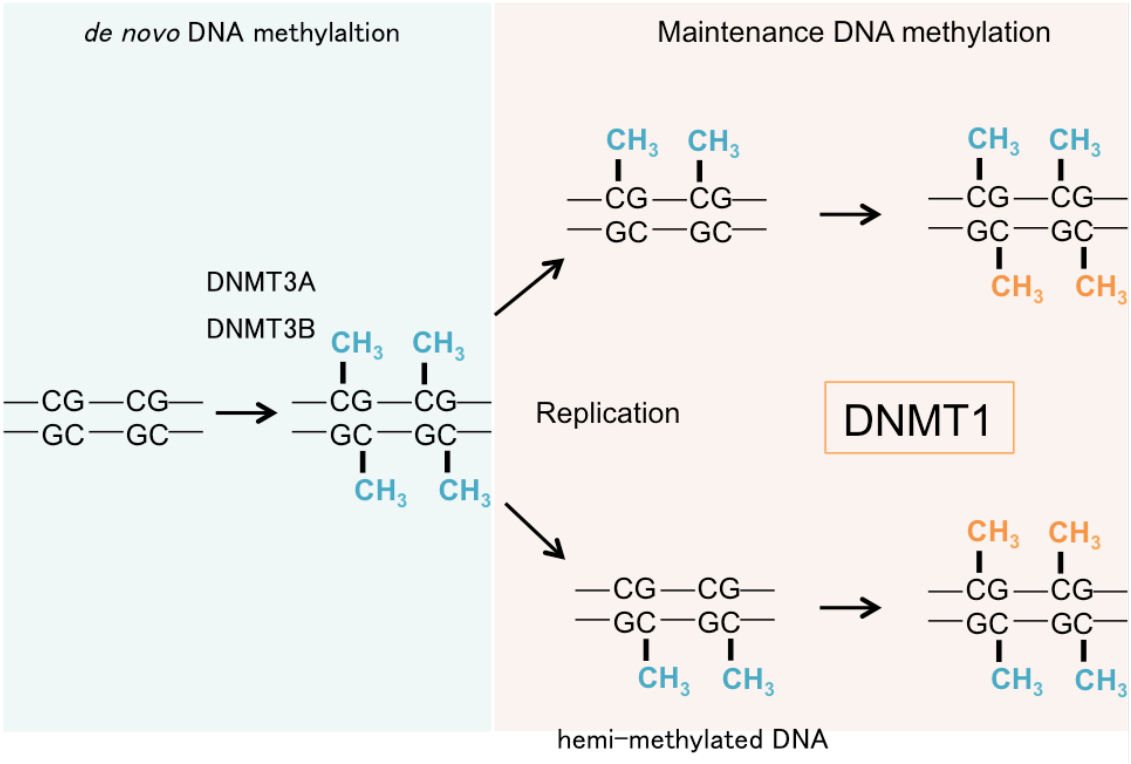

Figure 1.4 *De novo* DNA methylation and maintenance DNA methylation.

Once genome DNA methylation patterns are established by DNMT3A and DNMT3B, DNMT1 inherits these patterns by methylation toward hemi-methylated DNA during DNA replication.

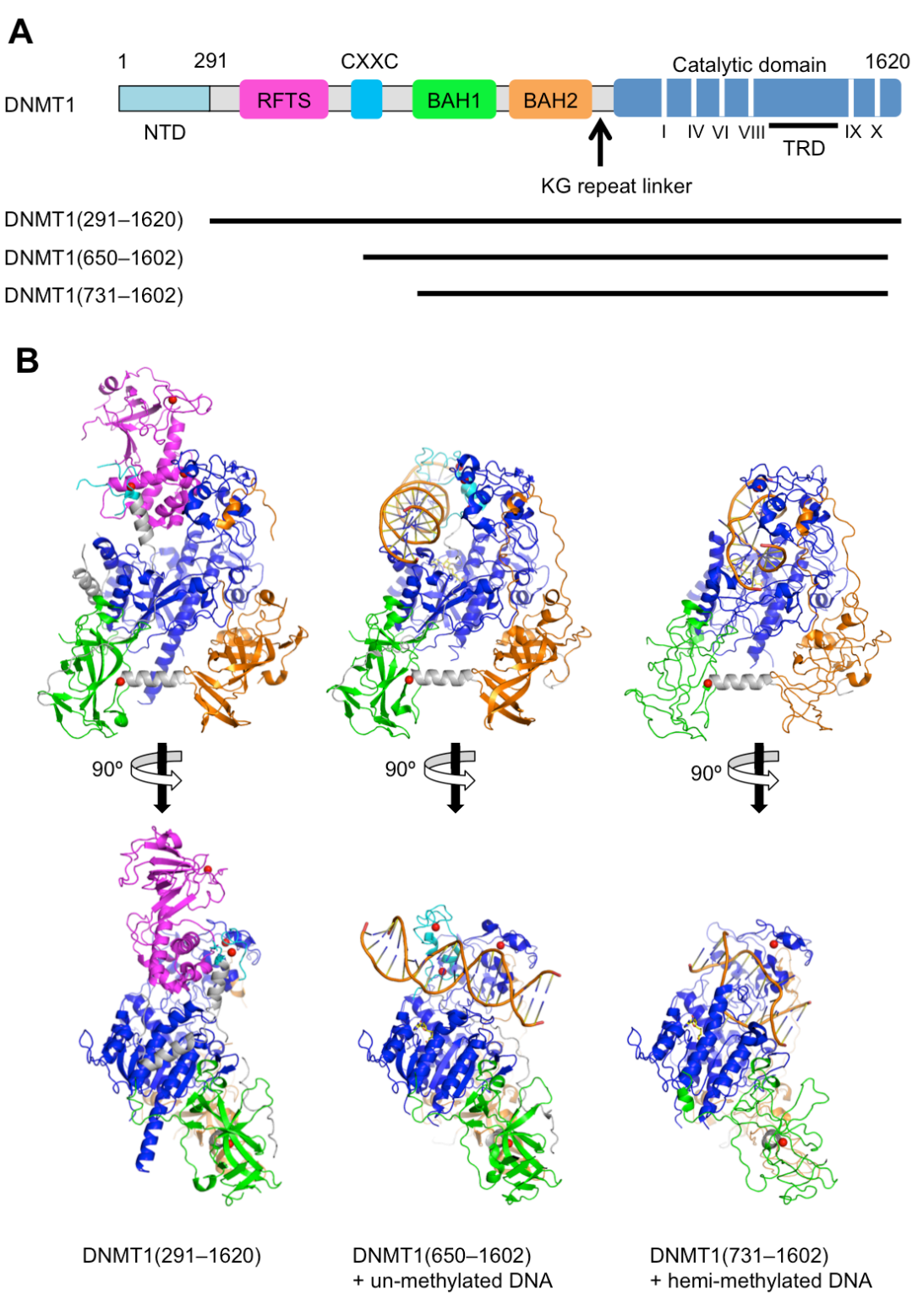

Figure 1.5 Crystal structures of DNMT1.

(A) Schematic illustrations of DNMT1. (B) The crystal structure models of DNMT1.

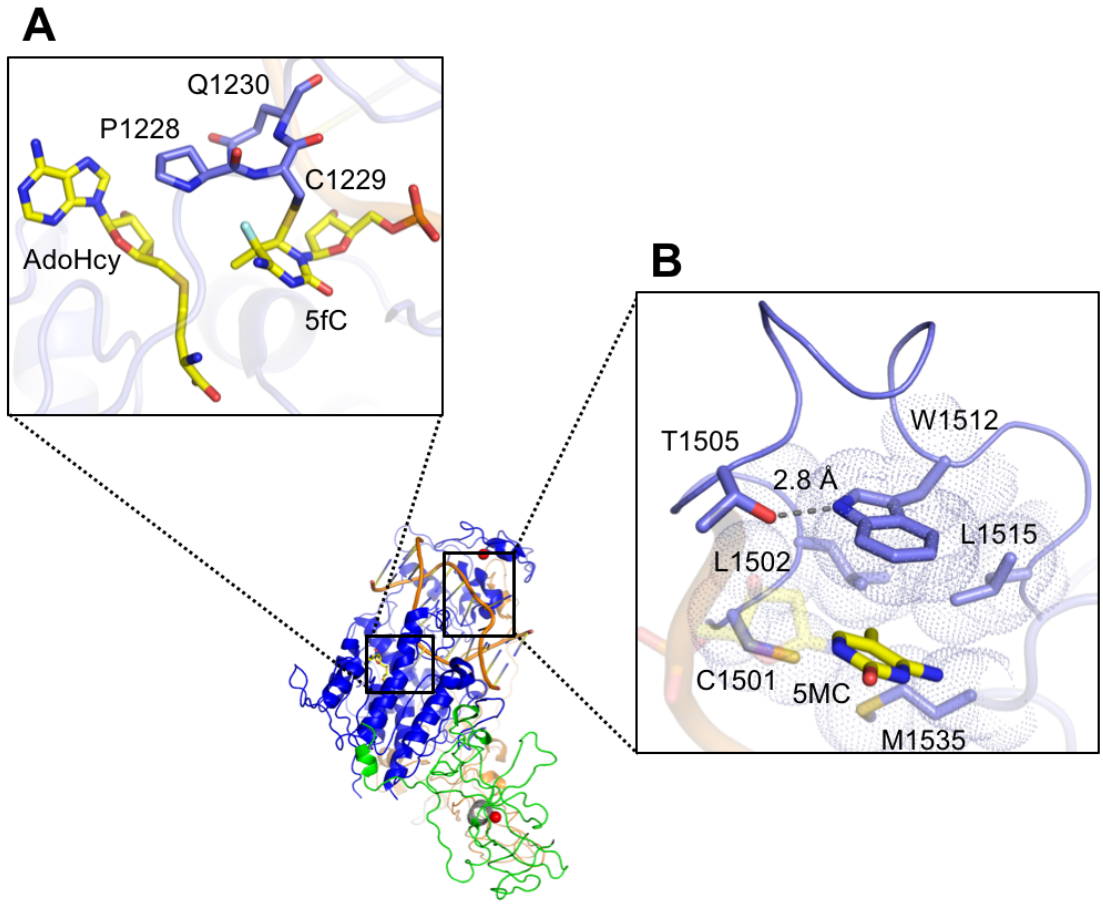

Figure 1.6 The binding of hemi-methylated DNA to mouse DNMT1.

Substrate binding in the crystal structure of mouse DNMT1(731–1602) in complex with hemi-methylated DNA containing 5-fluorocytosine (PDB accession number: 4DA4). (A) The catalytic center. C1229 forms a covalent bond to the sixth position of the flipped out 5-fluorocysotine (5fC), and the methyl group is transferred *S*-adenosyl-L-methionine (AdoMet) to 5fC. AdoMet is converted to *S*-adenosyl-L-homocysteine (AdoHcy). (B) The TRD loop. The side chains of C1501, L1502, W1512, L1515, and M1535 form a hydrophobic cage for recognition of the 5-methyl group of 5-methylcytosine (5MC) in hemi-methylated CpG. The indole ring of W1512 stacks the base of 5-methylcytosine, and W1512 has the hydrogen bond with T1505.

1.7 Purpose of this study

The multistep process of maintenance DNA methylation by DNMT1 probably contains (1) the release of the RFTS domain and the CXXC motif to catalytic pocket, (2) substrate recognition, (3) the transfer of a methyl group, and (4) the processive methylation or the release of substrate DNA form catalytic pocket. However, the essential property of DNMT1 regarding how DNMT1 retains structural stability of its 180 kDa molecule during these conformation change, and how DNMT1 possesses *de novo* DNA methylation activity keeping the balance of both activities remains unclear.

Previously, to identify residues which could contribute to structural stability of DNMT1, I evaluated the accession of DNA to catalytic pocket for DNMT1(291–1620) mutants that are impaired the hydrogen bonds the RFTS domain and the catalytic domain, and found that DNMT1(291–1620) which is replaced T1505 with alanine (DNMT1(291–1620)T1505A), which are impaired the hydrogen bond L593 and T1505, only scarcely bound to DNA (My master's thesis, 2014).

On the other hand, the O^{γ} of T1505 also has a hydrogen bond with the N^{ε} of this indole ring of W1512, although the side chains of C1501, L1502, L1515, and M1535 have no intermolecular hydrogen bond in both DNMT1(731–1602) in complex with hemi-methylated DNA and DNMT1(291–1620), and T1505, together with C1501, L1502, L1515, W1512 and M1535, is conserved in the TRD among known DNMT1 homologs in vertebrates. From the point of these views, T1505 could plays an important role in structural change of the RFTS domain and substrate recognition of DNMT1, but the function of T1505 is unclear.

In this study, to understand the further mechanism of DNA methylation activity of DNMT1, I analyzed the function and structure of DNMT1(291–1620)T1505A.

Chapter 2
Materials and methods

2.1 Preparation of recombinant DNMT1

cDNA of mouse DNMT1 harboring 291–1620 amino acid residues (DNMT1(291–1620)) and the mouse DNMT1(291–1620) that had its T1505 replaced with alanine (DNMT1(291–1620)T1505A) were subcloned into the EcoRI site of pFastBac-HTb (Invitrogen) with a GST-tag in the N-terminus. The baculoviruses of each fragment were constructed by Bac-to-Bac system, and amplified by three rounds in *Spodoptera frugiperda* (Sf9) cells, which were cultured in Grace's medium or Cosmedium containing 10% (v/v) fetal bovine serum at 27 °C. Baculoviruses harboring cDNA of DNMT1(291–1620) or DNMT1(291–1620)T1505A were infected into 1×10^6 Sf9 cells, and harvested 72 h after the infection (Takeshita *et al*., 2011).

The recombinant proteins were purified as described elsewhere (Vilkaitis *et al*., 2005; Takeshita *et al*., 2011; Berkyurek *et al*., 2014). The harvested cells were washed twice in Dulbecco's phosphate buffered saline. The cells were homogenized with a Dounce homogenizer in buffer containing 10% (w/v) glycerol, 3 mM $MgCl_2$, 0.1% (w/v) Nikkol, 1/500 (v/v) protease inhibitor cocktail (Nakalai Tesque), 2 mM DTT, and 20 mM Tris-HCl, pH7.6. Then, 5 M NaCl was added to a final concentration of 0.3 M NaCl, and the cells were homogenized again. The cell extract was centrifuged at 100,000 rpm for 15 min. The supernatant fraction was salted out by 40% (w/v) saturation with ammonium sulfate, and precipitates were dissolved in buffer A (0.35 M NaCl, 10% (w/v) glycerol, 0.01% (w/v) Nikkol, 1/1000 (v/v) 2-mercaptoethanol, 1/1000 (v/v) protease inhibitor cocktail, 20 mM imidazole, and 20 mM PIPES, pH 6.2). Samples were loaded onto tandem 5-ml HiTrap chelating HP columns (GE Healthcare), which were coordinated Ni^{2+} and equilibrated with buffer A, and recombinant DNMT1 was eluted with linear

gradient from 20 mM to 350 mM imidazole in buffer A. The main fractions were loaded onto glutathione-Sepharose column 4B (GE Healthcare) containing the equilibrium buffer (0.3 M NaCl, 0.01% (w/v) TritonX-100, 1 mM DTT, and 50 mM Tris-HCl, pH 7.0). The column was washed, and recombinant DNMT1 was eluted with the equilibrium buffer containing 10 mM reduced form of glutathione. The eluted fractions were dialyzed in the equilibrium buffer with 1 mM EDTA and PreScission Protease. After dialysis, samples were reloaded onto glutathione-Sepharose column 4B to trap GST-tags. Finally, purified DNMT1 was loaded onto a Superdex 200 (GE Healthcare) in 350 mM NaCl and 20 mM HEPES-Na (pH 7.4). For crystallization, DNMT1(291–1620)T1505A was further salted out by ammonium sulfate, dissolved, filtered through a 0.22-μm Ultrafree filter (Merck Millipore), and loaded onto a Superdex 200 in 350 mM NaCl and 20 mM HEPES-Na (pH 7.0). Purity of both DNMT1s was assessed by SDS-PAGE (Figure 2.1 for DNMT1(291–1620); Figure 2.2 for DNMT1(291–1620)T1505A) and by dynamic light scattering with a Zetasizer (Malvern). DNMT1(291–1620)T1505A was concentrated to 7 mg/ml for crystallization. The concentration of purified DNMT1s was determined from the absorbance at 280 nm with a NanoDrop 2000 spectrophotometer (Thermo Scientific).

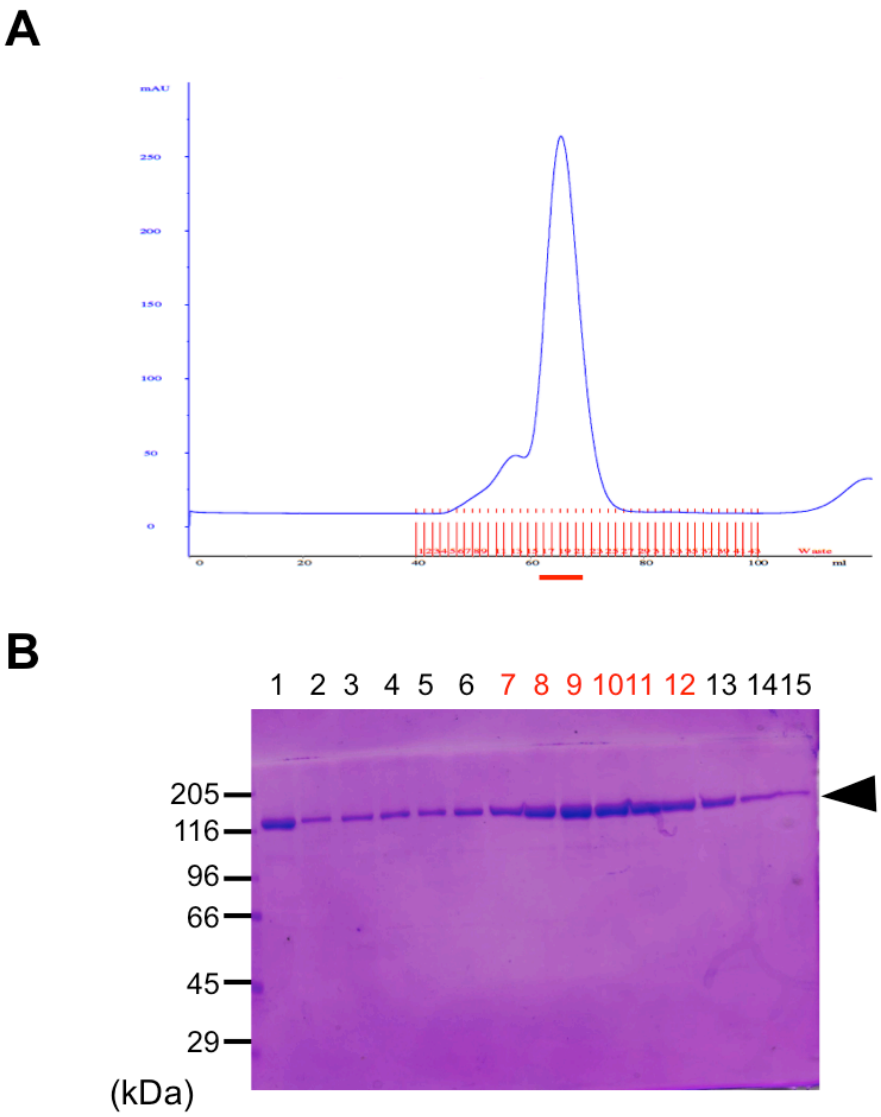

Figure 2.1 The chromatogram of final gel filtration chromatography and SDS-PAGE of DNMT1(291–1620).

(A) Chromatogram. (B) SDS-PAGE. The loaded sample (lane 1) and eluted samples (lanes 2–15) were subjected to 8% SDS-PAGE. The arrow shows the position of DNMT1(291–1620) (molecular mass is 150 kDa). The samples of lane 7–12 (red) were eluted at the position of the red line in (A), in which DNMT1(291–1620) forms a dimer.

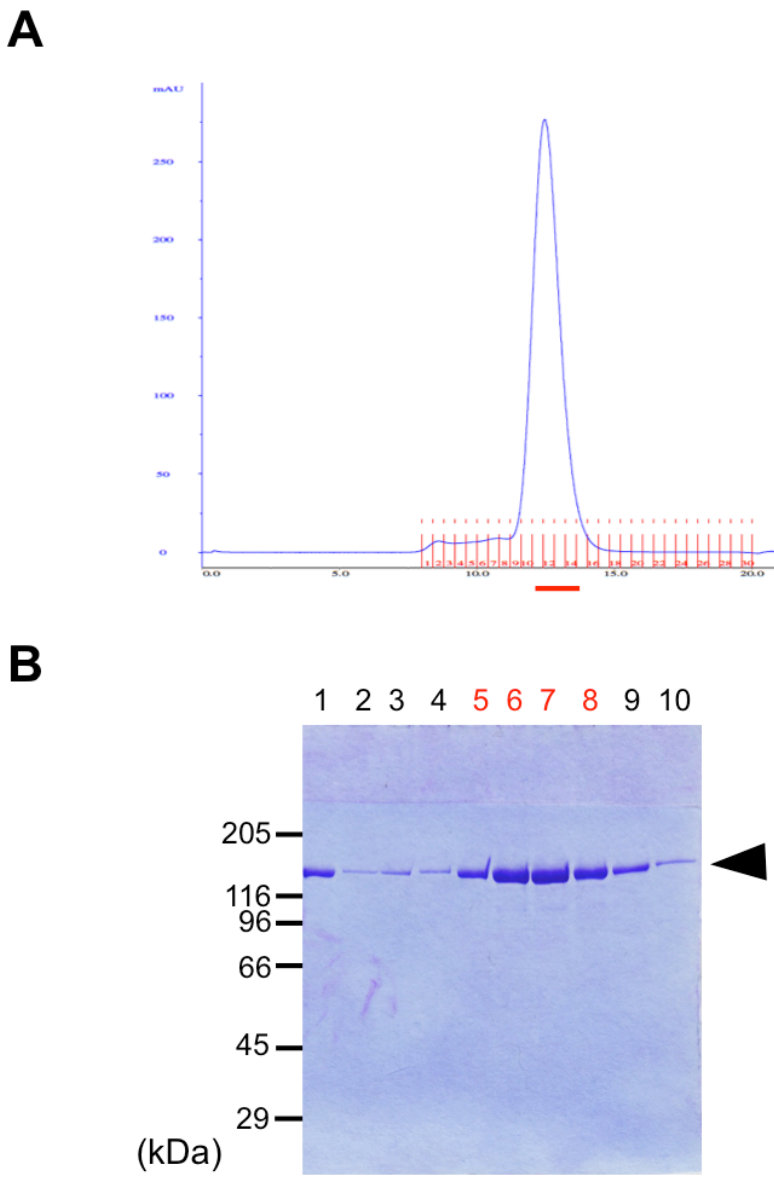

Figure 2.2 The chromatogram of final gel filtration chromatography for crystallization and SDS-PAGE of DNMT1(291–1620)T1505A.

(A) Chromatogram. (B) SDS-PAGE. The loaded sample (lane 1) and eluted samples (lanes 2–10) were subjected to 8% SDS-PAGE. The arrow shows the position of DNMT1(291–1620)T1505A (molecular mass is 150 kDa). The samples of lane 5–8 (red) were concentrated for crystallization. These samples were eluted at the position of the red line in (A), in which DNMT1(291–1620)T1505A forms a dimer.

2.2 Determination of DNA methylation activity

DNA methylation activity of DNMT1(291–1620) and DNMT1(291–1620)T1505A was determined as described elsewhere (Takeshita *et al.*, 2011). The reaction mixture was a total volume of 25 μl with 25 ng DNMT1(291–1620) or DNMT1(291–1620)T1505A, substrate DNA as described below (Table 2.1), 2.2 μM [^{3}H]-*S*-adenosyl-L-methionine (18 Ci/mmol) (PerkinElmer Life Sciences) and reaction buffer containing 5 mM EDTA, 2.7 M glycerol, 0.2 mM PMSF, 0.2 mM DTT, and 20 mM Tris-HCl (pH 7.4). The final concentration of substrate DNA in the reaction mixture was 33 nM for 42-bp DNA containing 12 hemi-methylated CpGs, 33 nM for 42-bp DNA containing 12 un-methylated CpGs, or 200 nM for 20-bp DNA containing 1CpG (Table 2.1). Reaction mixtures were incubated at the indicated temperatures for several different times, and reactions were stopped by adding 1.6 mM non-radioactive *S*-adenosyl-L-methionine. Then, the mixtures were incubated with Proteinase K at 55 ºC for 1 h and applied to DE81 filter disks (Whatman). The filters were washed three times with phosphate buffer (pH 7.0). The radioactivity was detected by a scintillation counter (Beckman LS-6500). DNA methylation activities were calculated as (mol C^3H_3 transferred to the substrate DNA/h/ mol DNMT1).

Table 2.1 Oligonulceotides for determination of DNA methylation activity

42-bp DNA containing 12 hemi-methylated CpGs
5′-GATCMGAMGAMGAMGAMGAMGAMGAMGAMGAMGAMGATC-3′
3′-CTAGGCTGCTGCTGCTGCTGCTGCTGCTGCTGCTGCTAG-5′
42-bp DNA containing 12 un-methylated CpGs
5′-GATCCGACGACGACGACGACGACGACGACGACGACGATC-3′
3′-CTAGGCTGCTGCTGCTGCTGCTGCTGCTGCTGCTGCTAG-5′
20-bp DNA containing one hemi-methylated CpG
5′-GAATGAGGCMICCTGCAAGC-3′
3′-CTTACTCCGGCGGACGTTCG-5′

(M indicates 5-methylcytosine, and I indicates inosine.)

2.3 Thermal stability assay

The thermal stability of DNMT1(291–1620) and DNMT1(291–1620)T1505A was monitored with ProteoStat dye (Enzo Life Sciences), which emits a strong red signal at around 600 nm upon binding to aggregated proteins.

To evaluate thermal stability of DNMT1s at 30 °C or 37 °C, 1 mg/ml DNMT1(291–1620) or DNMT1(291–1620)T1505A was dissolved in a 0.2 ml Hi-8 tube (TaKaRa) with a total volume of 25 µl mixtures containing 350 mM NaCl, 20 mM HEPES-Na (pH 7.0), and the ProteoStat dye. Then fluorescence was detected every 30 sec for 255 cycles in a real-time PCR system (Stratagene Mx3005p, Agilent Technologies).

To determine the midpoint temperature of denaturation (T_m), the same mixtures were gradually heated from 25 °C to 99 °C and fluorescence was detected with 2.98 °C/min in the same PCR system. These data were processed, and T_m was calculated by MxPro QPCR software (Agilent Technologies).

2.4 Crystallization

Initial crystals of DNMT1(291–1620)T1505A were obtained in previous crystallization conditions (Takeshita *et al*., 2011). Unlike the crystal of wild type DNMT1(291–1620), the crystals of DNMT1(291–1620)T1505A were needle shaped clusters and many crystalline nuclei generated in the above conditions. To decrease crystalline nuclei, temperature and the concentration of precipitant were decreased, and the concentration of NaCl was increased. Moreover, wider crystals were generated in crystallization cocktail containing sodium citrate tribasic dihydrate, which was identified by using the PEG/ion screen (Hampton Research inc).

DNMT1(291–1620)T1505A solution was mixed with an equal volume of reservoir solution containing 17% (w/v) PEG3350, 200 mM NaCl, 50 mM sodium citrate tribasic dihydrate, 20 mM tris(2-carboxyethyl)phosphine hydrochloride (TCEP-HCl), and 0.1 M Tris-HCl (pH 9.0), and this mixture was incubated at 298 K for 3.5 h in order to suppress forming crystal nuclei. Then, the crystals of DNMT1(291–1620)T1505A were grown at 293 K after incubation by the hanging drop vapor diffusion method (Figure 2.3). The reservoir solution was 500 µl of the crystallization cocktail. The crystals of DNMT1(291–1620)T1505A appeared after 5 days, and were grown into the maximum size for 20 days.

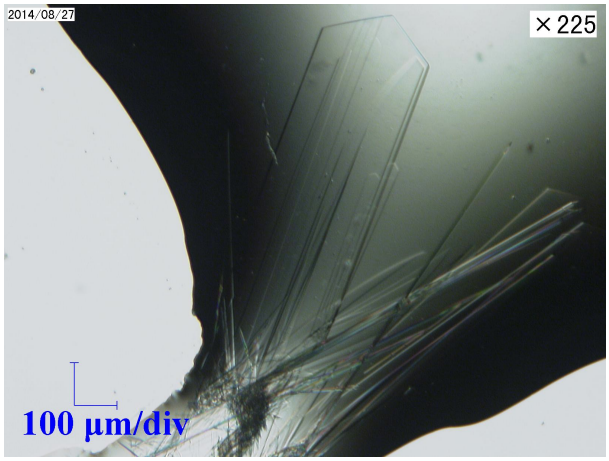

Figure 2.3 Crystals of DNMT1(291–1620)T1505A.

2.5 X-ray data collection and structure determination

The buffer containing 19% (w/v) PEG3350, 275 mM NaCl, 25 mM sodium citrate tribasic dihydrate, 10 mM TCEP-HCl, 10 mM HEPES-Na (pH 7.0), and 50 mM Tris-HCl (pH 9.0) were added to the drops containing the crystals of DNMT1(291–1620)T1505A. For cryo-protection, this mixture was gradually replaced the buffer containing 2% (w/v) PEG200 stepwise to 20% (w/v) PEG200. The crystals were lifted by LithoLoops (Protain Wave) and stored by flash freezing in liquid nitrogen.

All X-ray diffraction data were collected on the BL44XU beamline at SPring-8 (Harima, Japan) by an MX300HE detector (Rayonix) in liquid mist nitrogen. These data were processed and scaled with HKL2000 program (Otwinowski and Minor, 1997).

The initial phase was determined by molecular replacement with the program MOLREP (Vagin and Teplyakov, 2010) in the Collaborative Computing Project 4 (CCP4) suite (Winn *et al.*, 2011) by using the crystal structure of mouse DNMT1(291–1620) (PDB accession number: 3AV4) as a search model. The model building was performed by using *Coot* (Emsley *et al.*, 2010), and the structural refinement was carried out with the program REFMAC5 (Murshudov *et al*., 1997) in the CCP4 suite. All crystal structure figures were created using PyMOL (http://www.pymol.org/).

The coordinates and structure factor files of DNMT1(291–1620)T1505A have been deposited in Protein Data Bank (PDB) accession number 5WY1.

Chapter 3

Results

3.1 Maintenance DNA methylation activity of DNMT1(291–1620)T1505A

To examine whether DNMT1(291–1620)T1505A affects maintenance DNA methylation activity, the activity of DNMT1(291–1620) and DNMT1(291–1620)T1505A toward a 42-bp DNA containing 12 hemi-methylated CpGs was measured at 20 °C, 25 °C, 30 °C and 37 °C (Figure 3.1A). DNMT1(291–1620)T1505A possessed detectable maintenance DNA methylation activity, but its activity at 20 °C, 25 °C, 30 °C, and 37 ºC was lower than that of DNMT1(291–1620); the maintenance DNA methylation activity of DNMT1(291–1620) and DNMT1(291–1620)T1505A was 1.48 ± 0.59 and 0.68 ± 0.1 mol h^{-1} mol^{-1} at 20 °C, 1.82 ± 0.52 and 1.14 ± 0.18 mol h^{-1} mol^{-1} at 25 °C, 3.65 ± 1.38 and 1.90 ± 0.34 mol h^{-1} mol^{-1} at 30 °C, and 6.22 ± 1.31 and 0.95 ± 0.15 mol h^{-1} mol^{-1} at 37 ºC, respectively. The maintenance DNA methylation activity of DNMT1(291–1620) was increased in a temperature dependent manner as previous studies (Takeshita, *et al*., 2011; Berkyurek, *et al*., 2014). On the other hand, the maintenance DNA methylation activity of DNMT1(291–1620)T1505A at 37 °C (0.95 ± 0.15 mol h^{-1} mol^{-1}) was lower than that at 30 °C (1.90 ± 0.34 mol h^{-1} mol^{-1}), and was significantly about 6 times lower than the activity of DNMT1(291–1620) at 37 °C (6.22 ± 1.31 mol h^{-1} mol^{-1}). This reduction in DNMT1(291–1620)T1505A activity indicates that the temperature sensitivity of DNMT1(291–1620)T1505A is different from that of DNMT1(291–1620) in maintenance DNA methylation activity above 30 °C.

This reduction in maintenance DNA methylation activity of DNMT1(291–1620)T1505A at 37 °C was postulated to be either due to the following: (i) DNMT1(291–1620)T1505A linearly increases the DNA methylation amount, but its gradient is gentler

than that of DNMT1(291–1620); (ii) The DNA methylation amount of DNMT1(291–1620)T1505A reaches a plateau due to inactivation in a point during 1 h. To determine whether the reduction in the activity at 37 °C is due to (i) or (ii), the time course of DNA methylation toward a 20-bp DNA containing one hemi-methylated CpG was measured at 30 °C and 37 °C (Figure 3.1B, C). Both DNA methylation amount by DNMT1(291–1620) and DNMT1(291–1620)T1505A was continuously increased at 30 °C for at least 30 min (Figure 3.1B). However, at 37 °C, DNA methylation amount by DNMT1(291–1620)T1505A reached a plateau after about 12 min, while the amount by DNMT1(291–1620) was continuously increased (Figure 3.1C). These results indicate that DNMT1(291–1620)T1505A stopped DNA methylation reaction after several turnovers at 37 °C. Moreover, DNMT1(291–1620)T1505A did not restore its maintenance DNA methylation activity toward a 42-bp DNA containing 12 hemi-methylated CpGs even at 30 °C after pre-incubation at 37 °C for 30 min, 1 h, and 2 h, respectively (Figure 3.1D). On the other hand, both DNMT1(291–1620) and DNMT1(291–1620)T1505A possessed the maintenance DNA methylation activity at 30 °C after pre-incubation at 4 °C. These results demonstrate that the DNA methylation activity of DNMT1(291–1620)T1505A is irreversibly inactivated at 37 °C. Thus, the reduction in DNMT1(291–1620)T1505A activity at 37 °C was due to (ii).

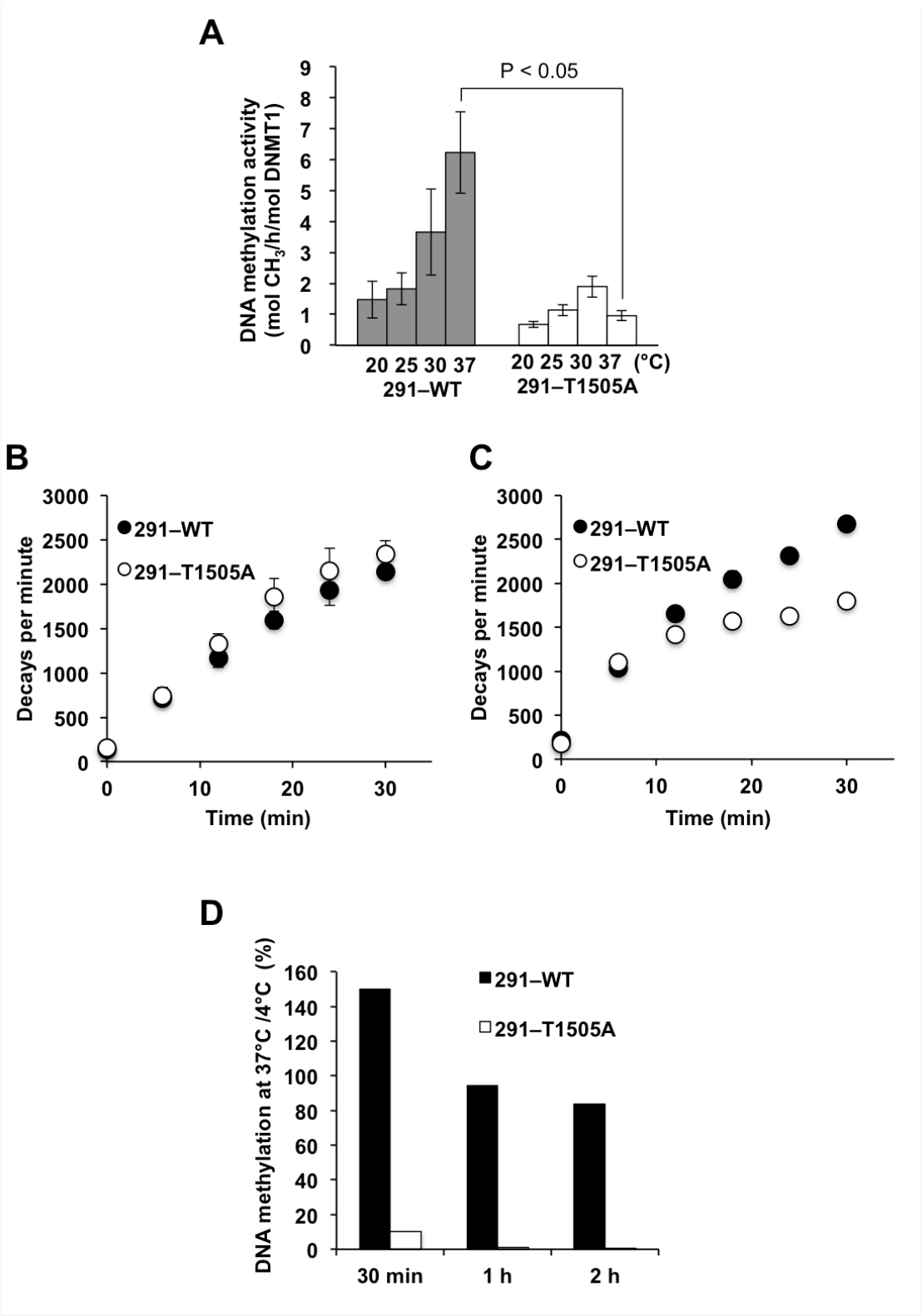
A
P < 0.05
DNA methylation activity
(mol CH3/h/mol DNMT1)
9
8
7
6
5
4
3
2
1
0
20 25 30 37
291–WT
20 25 30 37 (°C)
291–T1505A
B
3000
2500
2000
1500
1000
500
0
Decays per minute
291–WT
291–T1505A
0
10
20
30
Time (min)
C
3000
2500
2000
1500
1000
500
0
Decays per minute
291–WT
291–T1505A
0
10
20
30
Time (min)
D
DNA methylation at 37°C /4°C (%)
160
140
120
100
80
60
40
20
0
291–WT
291–T1505A
30 min
1 h
2 h

Figure 3.1 Distinct temperature sensitivity of DNMT1(291–1620) and DNMT1(291–1620)T1505A in maintenance DNA methylation activity.

(A) Maintenance DNA methylation activity of DNMT1(291–1620) (291–WT) (gray bars) and DNMT1(291–1620)T1505A (291–T1505A) (white bars) toward a 42-bp DNA containing 12 hemi-methylated CpGs at described temperatures. Averages ± S.E. (n = 3). (B–C) Time course of DNA methylation amount at 30 °C (B) and at 37 °C (C) toward a 20-bp DNA containing one hemi-methylated CpG site. Averages ± S.E. (n = 3). Filled and open circles represent DNMT1(291–1620) (291–WT) and DNMT1(291–1620)T1505A (291–T1505A), respectively. (D) Maintenance DNA methylation activity toward a 42-bp DNA containing 12 hemi-methylated CpGs at 30 °C with DNMT1s pre-incubated at 37 °C. After incubation of DNMT1(291–1620) (291–WT) (black) and DNMT1(291–1620)T1505A (291–T1505A) (white) at 37 °C or at 4 °C for the indicated time periods, each activity was determined at 30 °C and normalized as described at the vertical axis.

3.2 Thermal stability of DNMT1(291–1620)T1505A

DNMT1(291–1620)T1505A affected its maintenance DNA methylation activity in a temperature-dependent manner. The physical property change of DNMT1(291–1620)T1505A molecule by heat was postulated to be probably different from that of DNMT1(291–1620). To this end, thermal stability of both DNMT1s was monitored using ProteoStat dye, which emits a signal on binding to aggregated proteins. DNMT1(291–1620)T1505A drastically increased fluorescent signal at 37 ºC in a time-dependent manner, while DNMT1(291–1620) did not (Figure 3.2A). On the other hand, the fluorescent signal of DNMT1(291–1620)T1505A at 30 ºC was equivalent to that of DNMT1(291–1620) at 30 °C and at 37 °C. These indicate that DNMT1(291–1620)T1505A aggregates at 37 °C, resulting in the irreversible inactivation of DNMT1(291–1620)T1505A activity. Moreover, the fluorescent signal of DNMT1(291–1620) and DNMT1(291–1620)T1505A from 25 °C to 99 °C was plotted as the thermal-melt curve (Figure 3.2B). The fluorescence signal of DNMT1(291–1620) and DNMT1(291–1620)T1505A was increased from about 42 °C and 37 °C to 58 °C and 53 °C, respectively. The transition of temperature in aggregating was 16 °C for both DNMT1s. Figure 3.2C shows the derivative plots based on the raw fluorescent signal plots of Figure 3.2B. The midpoint temperature of denaturation (T_m), which is the temperature with the most rapid increase in fluorescence by aggregated protein, was determined as the first inflection point in Figure 3.2B. The T_m of DNMT1(291–1620) and DNMT1(291–1620)T1505A was estimated to be 49.6 °C and 44.5 °C, respectively. The T_m of DNMT1(291–1620)T1505A was about 5 °C lower than that of DNMT1(291–1620), indicated that T1505 plays a role in stabilizing the structure of DNMT1 molecule and this structural stability directly contributes to maintenance DNA methylation activity of DNMT1.

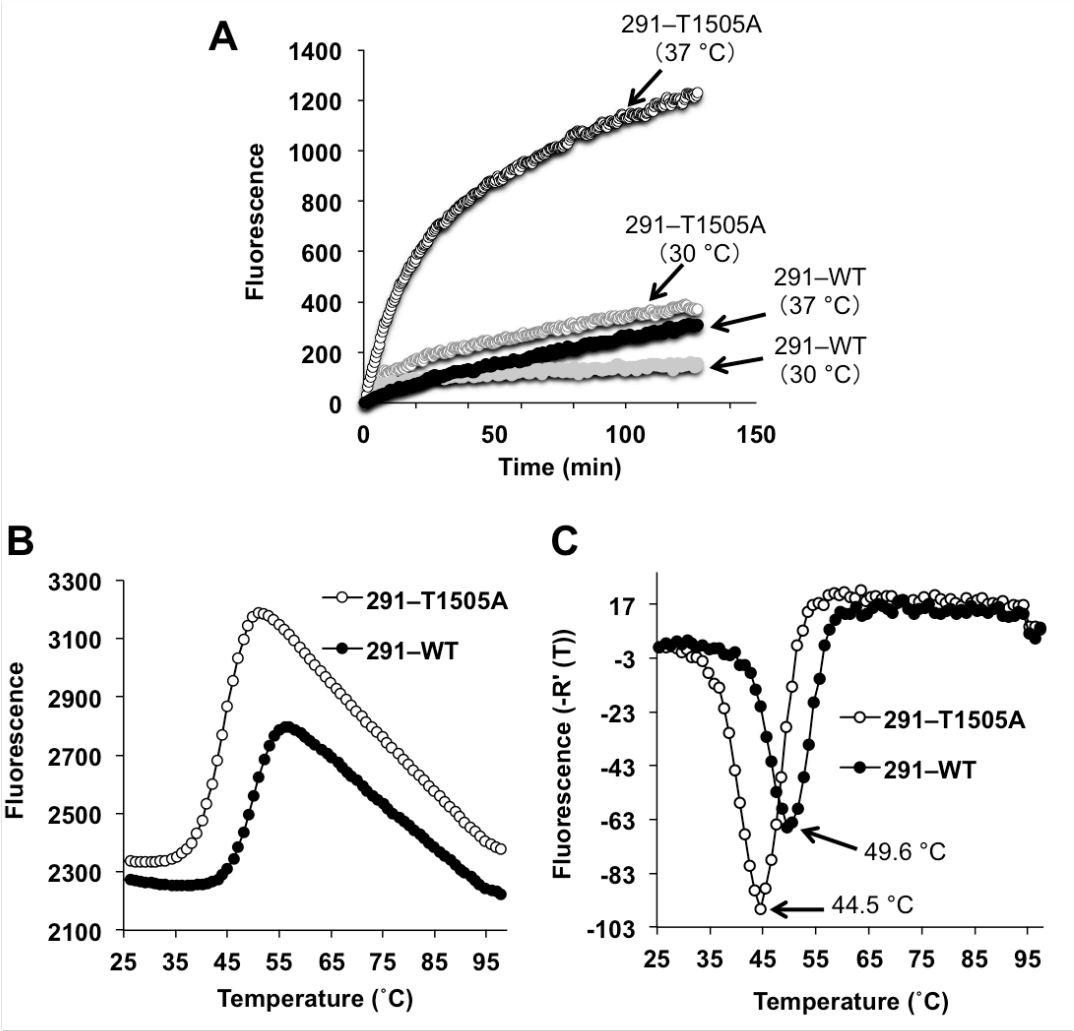

Figure 3.2 Thermal instability by T1505A mutation.

(A) Time-dependent aggregation of DNMT1(291–1620) (291–WT) and DNMT1(291–1620)T1505A (291–T1505A) at 30 °C and 37 °C. Data was detected as fluorescence signal by using ProteoStat dye. The filled and open circles show DNMT1(291–1620) and DNMT1(291–1620)T1505A at 30 °C (gray) and 37 °C (black), respectively. The arrows indicate each sample and temperature. (B) The thermal-melt curves of DNMT1(291–1620) (291–WT) (filled circles) and DNMT1(291–1620)T1505A (291–T1505A) (open circles) in a temperature dependent manner (25 ºC to 99 ºC). (C) The derivative plots based on (B). The arrows indicate the midpoint temperatures of denaturation (T_m)

3.3 The overall crystal structure of DNMT1(291–1620)T1505A

DNMT1(291–1620)T1505A aggregated at 37 ºC, but it almost retained maintenance DNA methylation activity at 30 ºC. Thus, to examine whether impairments of hydrogen bonds by T1505A mutation leads to the structural change in DNMT1 at below 30 ºC, the crystal structure analysis of DNMT1(291–1620)T1505A was performed.

The crystal structure of DNMT1(291–1620)T1505A was determined at 3.26 Å resolution (Table 3.1). This crystal belonged to the space group $P2_12_12$, and the cell dimensions of this crystal were a=135.1 Å, b= 97.9 Å, c=130.5 Å. These data were almost similar to those of the crystal of wild type DNMT1(291–1620) (Takeshita *et al.*, 2011). The phase of DNMT1(291–1620)T1505A was determined by the molecular replacement method using the crystal structure of DNMT1(291–1620) (PDB accession number: 3AV4) as a search model. The final model of DNMT1(291–1620)T1505A was refined to R_{work} and R_{free} of 20.3% and 26.3%, respectively (Table 3.2). Similar to DNMT1(291–1620), the crystal structure of DNMT1(291–1620)T1505A showed multi-domain structure, which contained the RFTS domain (328–600), the zinc-finger-like CXXC motif (650–695), two BAH domains BAH1 (758–897) and BAH2 (911–1103), and the catalytic domain (1125–1620), and its RFTS domain was held in the DNA-binding pocket (Figure 3.3A, B) (described next section). The amino acid residues (291–356, 394–404, 606–616, 642–652, 666–687, 711–713, 745–746, 852–864, 957–963, 982–988, 1109–1137, and 1613–1620) were disordered in both crystal structures of DNMT1(291–1620) and DNMT1(291–1620)T1505A. Therefore, some residues in the CXXC motif and the KG repeat linker (1112–1124) were not assigned. The crystal structure models of DNMT1(291–1620) and DNMT1(291–1620)T1505A were superimposed well (Figure 3.3C). The root mean square deviation (r.m.s.d.) between these crystal structures were calculated by the SUPERPOSE (Krissinel and Henrick, 2004) in the CCP4 suite. The r.m.s.d. values of the main chains and the side chains in both the crystal structures were

0.302 Å and 0.505 Å, respectively. The percentages in the Ramachandran plots of DNMT1(291–1620)T1505A were 90% (favored regions), 8% (additionally allowed regions), and 2% (Outliers), respectively (Table 3.2; Figure 3.4). As a result, the overall crystal structure of DNMT1(291–1620)T1505A was almost similar to those of wild type DNMT1(291–1620) (PDB accession number: 3AV4).

Table 3.1 X-ray diffraction data collection statistics of the DNMT1(291–1620)T1505A

Data collection	
Diffraction source	BL44XU, SPring-8
Wavelength (Å)	0.90000
Detector	MX300HE
Space group	$P2_12_12$
Cell dimensions	
a, *b*, *c* (Å)	135.1, 97.9, 130.5
Resolution range (Å)	50.00-3.26 (3.32-3.26)
Total No. of reflections	118,782
No. of unique reflections	26,720
Completeness (%)	97.5 (96.4)
Redundancy	4.4 (4.4)
$\langle I/\sigma(I)\rangle$	6.6 (1.6)
Overall B factor from Wilson plot ($Å^2$)	73.5

Data for the highest-resolution shell are given in parentheses.

Table 3.2 Refinement statistics of DNMT1(291–1620)T1505A

Refinement	
R_{work}/R_{free}	20.3/26.3
No. atoms	
Protein	9108
Ion	4
Water	23
R.m.s. deviations	
Bonds (Å)	0.01
Angles (°)	1.42
Average B-factors (Å^2)	
Protein	87.0
Ramachandran plot	
Favored regions (%)	90
Additionally allowed regions (%)	8
Outliers (%)	2

$R_{work} = \Sigma_{h\,k\,l}\,||F_{obs}|-|F_{calc}||/\Sigma_{h\,k\,l}\,|F_{obs}|$, where $|F_{obs}|$ and $|F_{calc}|$ are observed and calculated structure factor amplitudes, respectively.

R_{free} is equivalent to R_{work} except that 5% of the total reflections are set aside for an unbiased test of the progress of the refinement.

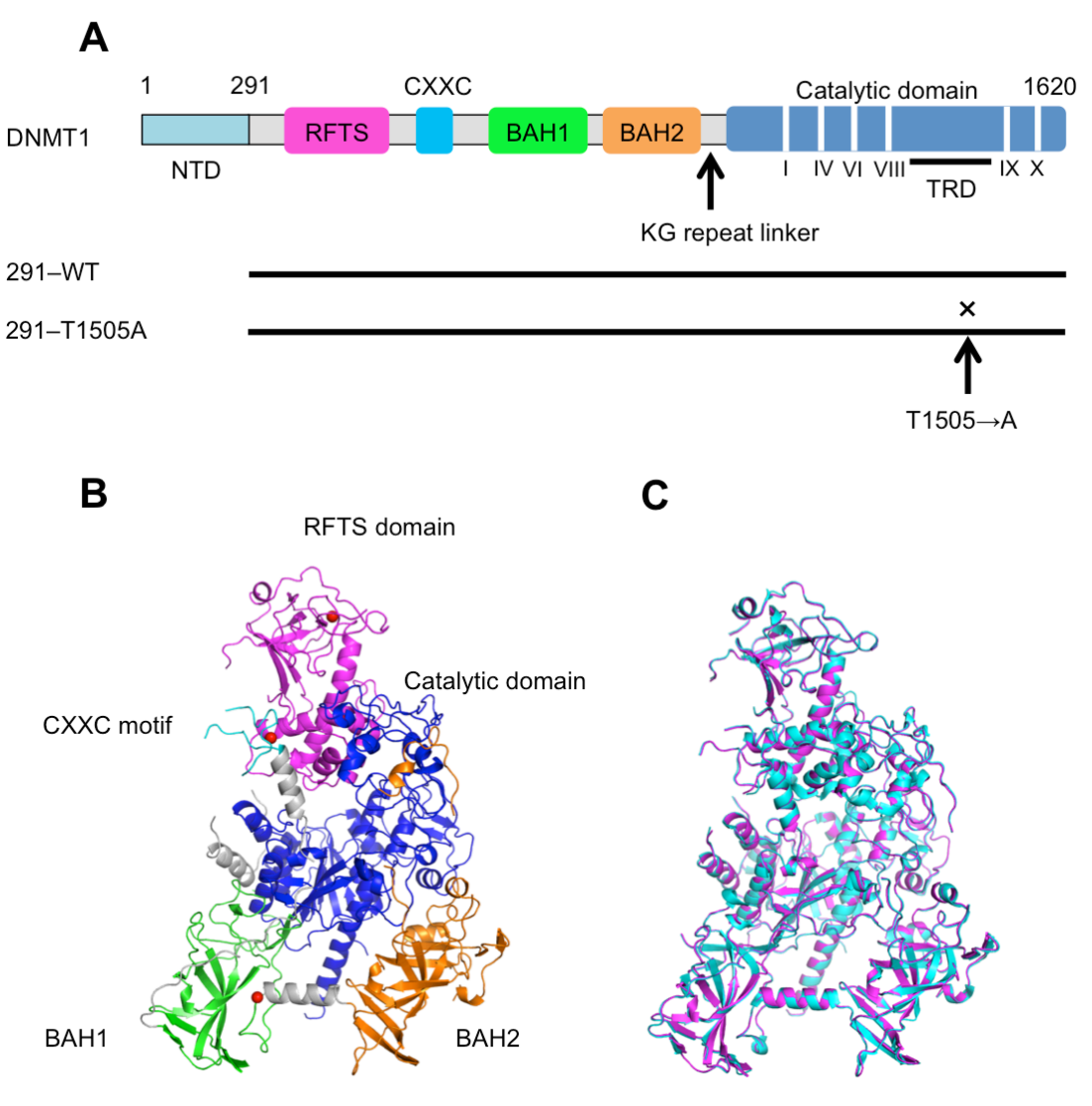

Figure 3.3 The crystal structure of DNMT1(291–1620)T1505A

(A) Schematic illustration of DNMT1s in this study. The below lines show constructions of DNMT1(291–1620) (291–WT) and DNMT1(291–1620)T1505A (291–T1505A), and 291–T1505A harbors a point mutation of T1505 to alanine in the TRD loop (cross mark). (B) The crystal structure of DNMT1(291–1620)T1505A. The RFTS domain (magenta), the CXXC motif (cyan), the BAH1 domain (green), the BAH2 domain (orange), and the catalytic domain (blue) are shown. (C) Superimposition of the crystal structures of DNMT1(291–1620) (cyan) (PDB accession number: 3AV4) and DNMT1(291–1620)T1505A (magenta).

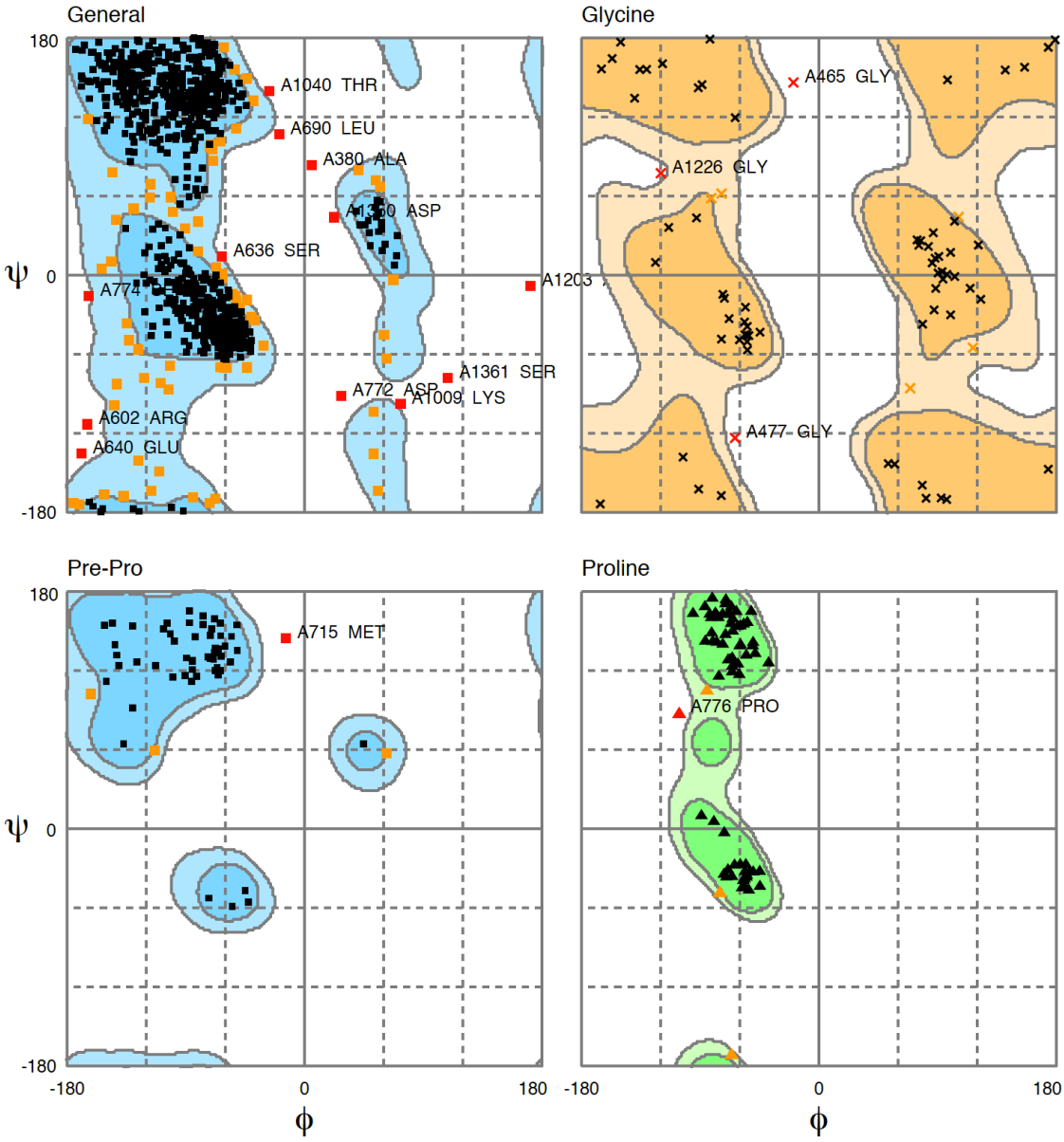

Figure 3.4 Ramachandran plots of the crystal structure of DNMT1(291–1620)T1505A

This analysis was performed by the RAMPAGE (Lovell *et al.*, 2003). Diagrams show the phi torsion angle and the psi torsion angle for general case (left above), for Glycine (right above), for Pre-Proline (left bottom), and for Proline (right bottom). Dark colors show favored regions, and light colors show additionally allowed regions.

3.4 The structural properties of DNMT1(291–1620)T1505A

The crystal structure of DNMT1(291–1620) has the hydrogen bond between the O^{γ} of T1505 and the N^{ε} of W1512 (2.8 Å) (PDB accession number: 3AV4; Figure 3.5A). It is reasonable to postulate that the impairment of this hydrogen bond likely affects the conformation of the indole ring of W1512. However, this hydrogen bond was impaired with the spatial orientation of W1512 retained in the crystal structure of DNMT1(291–1620)T1505A (Figure 3.5B). The σ_A-weighted $2F_{obs}$ - F_{calc} electron density map of the crystal structure of DNMT1(291–1620)T1505A did not show the map of the side chain of T1505 (Figure 3.5C). Therefore, T1505 certainly was replaced with alanine in DNMT1(291–1620)T1505A. The distance between the C^{β} of the alanine at 1505 and the N^{ε} of W1512 was about 3.8 Å. This distance change suggests that the side chain of W1512 in DNMT1(291–1620)T1505A could increase flexibility compared with that in DNMT1(291–1620).

C1501, L1502, L1515, and M1535 of the crystal structure of DNMT1(291–1620)T1505A were assigned as those of the crystal structure of DNMT1(291–1620). The conformation of these side chains was similar in both crystal structures (Figure 3.6). DNMT1(291–1620)T1505A may retain the ability to create the hydrophobic cage for recognition of the 5-methyl group of hemi-methylated CpG.

In the crystal structure of DNMT1(291–1620), the O^{γ} of T1505 also forms another hydrogen bond with the main chain carbonyl oxygen of L593 from the RFTS domain (2.8 Å) (PDB accession number: 3AV4; Figure 3.7A). This hydrogen bond, together with other hydrogen bonds between the RFTS domain and the catalytic domain, anchors the RFTS domain in the DNA-binding pocket (Takeshita, *et al*., 2011; Berkyurek, *et al*., 2014). Similar to the crystal structure of DNMT1(291–1620), the RFTS domain in the crystal structure of DNMT1(291–1620)T1505A also inserted into its DNA-binding pocket (Figure 3.3B, C) in spite of the lack of a hydrogen bond between T1505 and L593

(Figure 3.7B). The distance between the C^{β} of the alanine at 1505 and the main chain carbonyl oxygen of L593 was about 3.9 Å, but the amino acid residues around L593 were similar conformation as those of DNMT1(291–1620). In addition, the other hydrogen bonds between the RFTS domain and the catalytic domain in the crystal structure of DNMT1(291–1620)T1505A were the interactions between the O^{ε} of E531 and the main chain nitrogen of K1537 (3.0 Å), the O^{δ} of D532 and the N^{η} of R1576 (2.9 Å), and the O^{ε} of D554 and the main chain nitrogen of S1495 (3.1 Å), respectively. These hydrogen bonds were similar positions as those in the crystal structure of DNMT1(291–1620) (Figure 3.7C, D).

Taken together, the position of the RFTS domain and the structure of the hydrophobic cage for recognition was retained in DNMT1(291–1620)T1505A, its maintenance DNA methylation activity could be evaluated at below 30 ºC without problems.

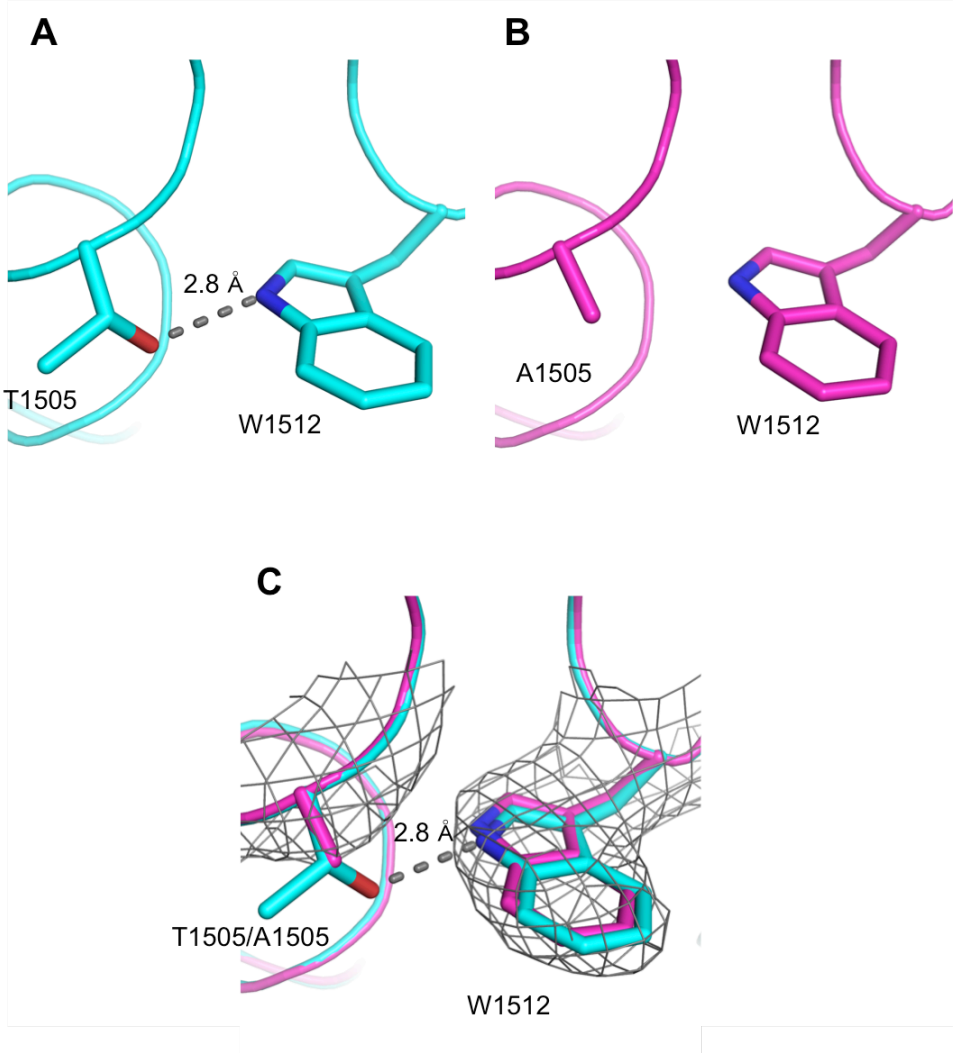

Figure 3.5 The impairment of the hydrogen bond between T1505 and W1512 in the crystal structure of DNMT1(291–1620)T1505A

(A) The hydrogen bond between the O^{γ} of T1505 and the N^{ε} of W1512 in the crystal structure of DNMT1(291–1620) (PDB accession number: 3AV4). The dotted line shows the hydrogen bond. (B) Replacement of T1505 with alanine in the crystal structure of DNMT1(291–1620)T1505A. (C) Superimposition of DNMT1(291–1620) (cyan) and DNMT1(291–1620)T1505A (magenta) with the σ_A-weighted $2F_{obs}$ - F_{calc} map of the crystal structure of DNMT1(291–1620)T1505A (contoured at 1.0 σ). The dotted line shows the hydrogen bond in DNMT1(291–1620).

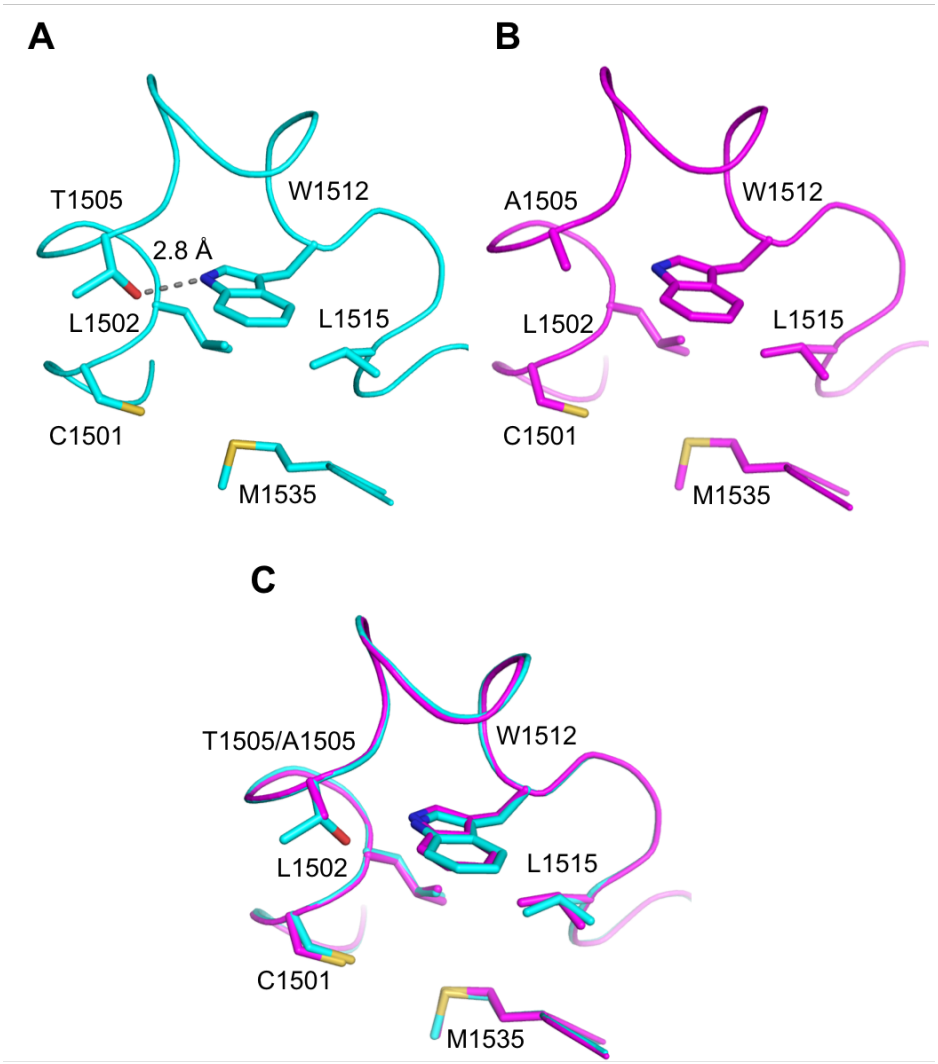

Figure 3.6 Superimposition of the TRD loops in the crystal structure of DNMT1 (291–1620) and DNMT1(291–1620)T1505A.

(A) The TRD loop of DNMT1(291–1620) (PDB accession number: 3AV4). The dotted line shows the hydrogen bond. (B) The TRD loop of DNMT1(291–1620)T1505A. (C) Superimposition of the TRD loops of DNMT1 (291–1620) (PDB accession number: 3AV4) (cyan) and DNMT1(291–1620)T1505A (magenta). The amino acid residues involved in holding the 5-methyl group (C1501, L1502, L1515, W1512 and M1535) (Song *et al*., 2012) in DNMT1(291–1620)T1505A have similar conformations as those in DNMT1 (291–1620).

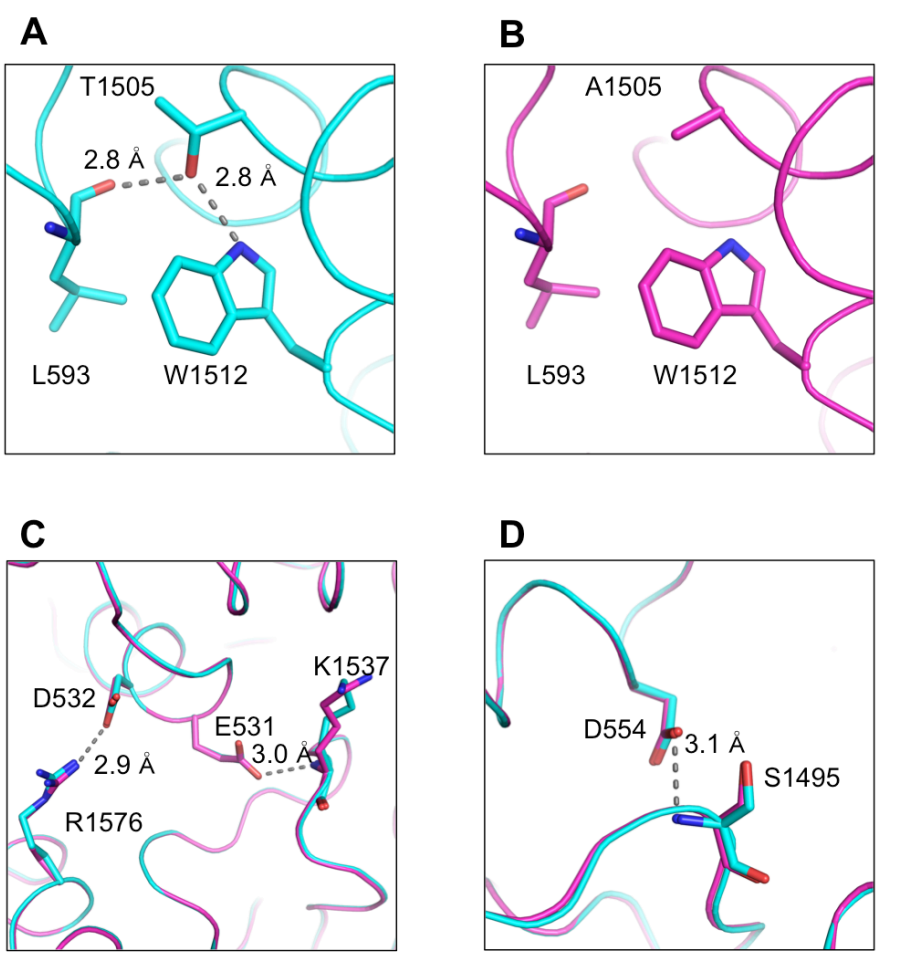

Figure 3.7 The hydrogen bonds between the RFTS domain and the catalytic domain.

(A) The O^{γ} of T1505 also forms another hydrogen bond with the main chain carbonyl oxygen of L593 from the RFTS domain in the crystal structure of DNMT1(291–1620) (PDB accession number: 3AV4). Dotted lines indicate hydrogen bonds. (B) The hydrogen bond between L593 and T1505 is impaired in the crystal structure of DNMT1(291–1620)T1505A. (C–D) Superimposition of the other hydrogen bonds between the RFTS domain and the catalytic domain in the crystal structures of DNMT1(291–1620) (cyan) and DNMT1(291–1620)T1505A (magenta). Dotted lines indicate hydrogen bonds in DNMT1(291–1620)T1505A.

3.5 *De novo* DNA methylation activity of DNMT1(291–1620)T1505A

DNMT1 also possesses significant *de novo* DNA methylation activity *in vitro*. To assess the influence of T1505A mutation on *de novo* DNA methylation activity by using maintenance DNA methylation activity of DNMT1(291–1620)T1505A as positive control (Figure 3.1A), the activity of DNMT1(291–1620)T1505A toward a 42-bp DNA containing 12 un-methylated CpGs was measured at 20 °C, 25 °C, 30 °C and 37 °C (Figure 3.8A). The *de novo* DNA methylation activity of DNMT1(291–1620) and DNMT1(291–1620)T1505A was 0.12 ± 0.05 and 0.01 ± 0.004 mol h^{-1} mol^{-1} at 20 °C, 0.25 ± 0.06 and 0.03 ± 0.01 mol h^{-1} mol^{-1} at 25 °C, 0.64 ± 0.05 and 0.08 ± 0.01 mol h^{-1} mol^{-1} at 30 °C, and 1.23 ± 0.14 and 0.04 ± 0.003 mol h^{-1} mol^{-1} at 37 °C, respectively. The *de novo* DNA methylation activity of DNMT1(291–1620)T1505A was significantly lower than that of DNMT1(291–1620) even at below 30 °C, in which DNMT1(291–1620)T1505A retains its structural stability. The relative activity of DNMT1(291–1620) to DNMT1(291–1620)T1505A showed that the rate of decline for *de novo* DNA methylation activity was higher than that for maintenance DNA methylation activity (Figure. 3.8B; Table 3.3). Figure 3.8C and Table 3.4 shows the ratio of methylation activity toward hemi-methylated DNA divided by methylation activity toward un-methylated DNA for DNMT1(291–1620) and DNMT1(291–1620)T1505A, respectively. The ratio of DNMT1(291–1620) and DNMT1(291–1620)T1505A was 25 ± 11.6 and 77.5 ± 35.8 at 20 °C, 7.4 ± 0.8 and 40 ± 8.3 at 25 °C, 5.4 ± 1.6 and 23.7 ± 2.3 at 30 °C, and 5.0 ± 1.0 and 26.7 ± 2.5 at 37 °C, respectively. Thus, the specificity for hemi-methylated DNA of DNMT1(291–1620)T1505A activity was increased as compared with that of wild type DNMT1(291–1620), implying that T1505 plays a role in recognition of un-methylated DNA.

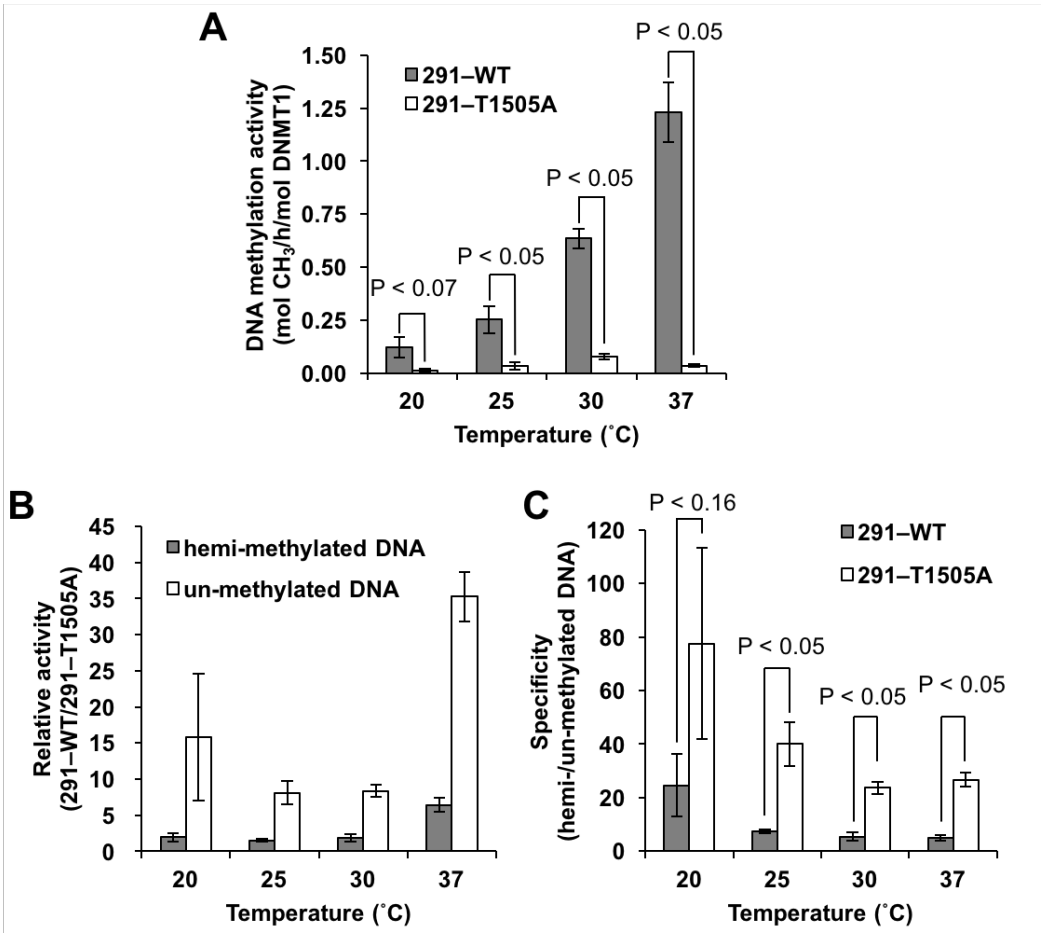

Figure 3.8 Reduction in *de novo* DNA methylation activity by T1505A mutation.

(A) *De novo* DNA methylation activity of DNMT1(291–1620) (291–WT) (gray bars) and DNMT1(291–1620)T1505A (291–T1505A) (white bars) toward a 42-bp DNA containing 12 un-methylated CpGs at described temperatures. Averages ± S.E. (n = 3). (B) Relative activities of DNMT1(291–1620) (291–WT) to DNMT1(291–1620)T1505A (291–T1505A). These ratios were calculated according to data of Figure 3.1A for hemi-methylated DNA (gray bars) and Figure 3.8A for un-methylated DNA (white bars). (C) Substrate specificity of DNMT1(291–1620) (291–WT) (gray bars) and DNMT1(291–1620)T1505A (291–T1505A) (white bars). These were calculated as the ratio of the data of methylation activity toward hemi-methylated DNA divided by methylation activity toward un-methylated DNA.

Table 3.3 Relative activity (291–WT/291–T1505A)

Temperature (ºC)	20	25	30	37
hemi/hemi	2.0 ± 0.6	1.5 ± 0.2	1.9 ± 0.5	6.4 ± 1.0
un/un	15.8 ± 8.8	8.1 ± 1.6	8.4 ± 0.8	33.7 ± 3.0

Table 3.4 Substrate specificity (hemi-/un-methylated DNA)

Temperature (ºC)	20	25	30	37
291–WT	25 ± 11.6	7.4 ± 0.8	5.4 ± 1.6	5.0 ± 1.0
291–T1505A	77.5 ± 35.8	40 ± 8.3	23.7 ± 2.3	26.7 ± 2.5

Chapter 4
Discussion

In previous study, our group determined the crystal structure of mouse DNMT1(291–1620), which is deleted the NTD (Takeshita *et al*., 2011). DNA methylation activity of DNMT1(291–1620) is equivalent to that of the full-length DNMT1, and therefore the NTD does not affect maintenance DNA methylation *in vitro* and *in vivo* (Vilkaitis *et al.*, 2005; Garvilles *et al.,* 2015). Since the crystal structure of full-length DNMT1 has not been reported, DNMT1(291–1620) was adopted for the positive control in this study. Thus, I prepared the same length recombinant mouse DNMT1(291–1620)T1505A, and performed its crystal structure analysis. This crystal structure showed the elimination of two hydrogen bonds between T1505 and L593 and between T1505 and W1512, but these eliminations did not drastically lead to the conformational changes of the RFTS domain and the side chain of W1512. To examine the role of T1505 to DNA methylation activity, I performed biochemical experiments, and showed the mainly two results: (1) DNMT1(291–1620)T1505A aggregated at physiological temperature and its DNA methylation activity was inactivated. (2) DNMT1(291–1620)T1505A increased the substrate specificity for hemi-methylated DNA. I found that T1505 plays a role in the mechanism of DNMT1 activity through the structural stability and contributes to possessing *de novo* DNA methylation activity. Thus, I suggested that the structure of DNMT1 may be supported by the trade-off between structural stability at physiological temperature and the substrate specificity of DNMT1 activity for hemi-methylated DNA through T1505.

4.1 The maintenance DNA methylation mechanism through the structural stability of DNMT1 molecule

The structural change of DNMT1(291–1620)T1505A was mainly the loss of two hydrogen bonds between T1505 and W1512 and between T1505 and L593 (Figure 3.7A, B). Either of these impairments would cause inactivation of DNA methylation activity at 37 ºC by the structural instability of DNMT1(291–1620)T1505A (Figure 3.1; Figure 3.2). The RFTS domain in wild type DNMT1(291–1620) has to be released from the catalytic pocket in binding of substrate DNA to the catalytic pocket during DNA methylation, implying that impairments of the hydrogen bonds between the RFTS domain and catalytic domains make it easy to remove the RFTS domain from the catalytic pocket (Takeshita *et al*., 2011; Syeda *et al*., 2011; Berkyurek *et al*., 2014). In fact, the DNMT1(291–1620) mutants with E531A/D532A and D554A that are impaired the hydrogen bonds between the RFTS and catalytic domains, and DNMT1(602–1620) lacking the RFTS domain do not show significant reduction in the maintenance DNA methylation activity at 37 °C, in which these activities are higher than those at 30 ºC (Berkyurek *et al*., 2014). Release of the RFTS domain does not lead to reduction in maintenance DNA methylation activity of DNMT1 in a temperature-dependent manner. Therefore, the impairment of the hydrogen bond between T1505 and L593 does not probably cause inactivation of DNMT1(291–1620)T1505A activity at 37 ºC. Thus, I judged that the impairment of the hydrogen bond between T1505 and W1512 causes inactivation through the structural instability of DNMT1(291–1620)T1505A at 37 ºC. It is reasonable to speculate that the aggregation of DNMT1(291–1620)T1505A starts from the surrounding region of the W1512, and this destabilization directly causes reduction in maintenance DNA methylation activity of DNMT1(291–1620)T1505A at 37 ºC (Figure 3.1). I suggest that the mechanism via maintaining the structural stability of DNMT1 molecule by T1505 is essential for DNA methylation activity of DNMT1.

4.2 Conservation of T1505 and W1512 among eukaryotic DNMT1 homologs

The conservation of T1505 and W1512 is assessed in alignment of amino acid sequences around the TRD loops in eukaryotic DNMT1 homologs (Figure 4.1A). The amino acid sequences of the TRD loops are completely conserved in vertebrate DNMT1s. In addition, the crystal structure of human DNMT1 comprising amino acid residues 351–1600 (human DNMT1(351–1600)) was reported (Zhang *et al*., 2015). T1503 and W1510 of human DNMT1 correspond to T1505 and W1512 of mouse DNMT1, and the O^{γ} of T1503 forms a hydrogen bond with the N^{ε} of W1510 (Figure 4.1B) (PDB accession number: 4WXX). The hydrogen bond between the conserved threonine and tryptophan is probably structurally conserved among vertebrate DNMT1s.

Apis mellifera, *Arabidopsis thaliana*, and *Orza sativa* possess DNMT1A (Wang *et al*., 2006; Kucharski *et al*., 2008), MET1 (Goll and Bestor, 2005; Du *et al*., 2015; Niederhuth and Schmitz, 2016), and MET1B (Yamauchi *et al*., 2014), respectively (Figure 4.1A). Among these DNMT1 homologs, the corresponding threonine of T1505, together with the corresponding hydrophobic amino acid residues of C1501, L1502, L1515, W1512, and M1535 for harboring 5-methyl group in hemi-methylated CpG, is completely conserved. *Neurospora crassa* possesses the sole DNA (cytosine-5) methyltranseferase DIM-2, which probably methylates hemi-methylated DNA (Tamaru and Selker, 2001; Goll and Bestor, 2005; Du *et al*., 2015), and T1146 and W1153 are just conserved, respectively.

These conservations imply that the conserved threonine and tryptophan among eukaryotic DNMT1 homologs could commonly be indispensable to maintaining the structural stability of each homolog molecule to gain DNA methylation activity.

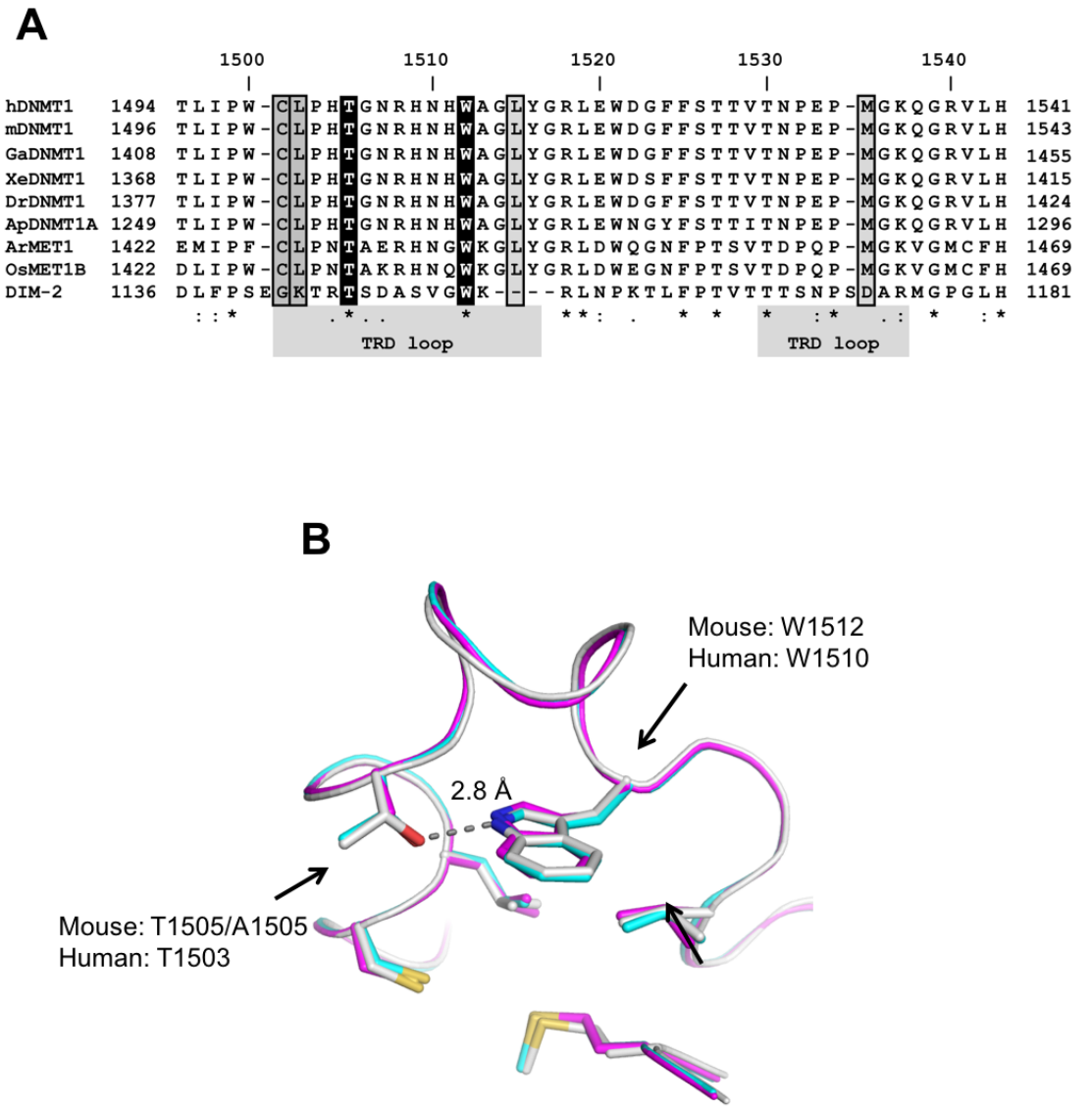

Figure 4.1 Conservation of T1505 and W1512.

(A) Amino acid sequence alignment around the TRD loops of DNMT1 homologs by the Clustal Omega (Goujon *et al*., 2010; Sievers *et al*., 2011; McWilliam *et al*., 2013). hDNMT1: human Dnmt1 (UniProt accession number: P26358), mDNMT1: mouse DNMT1 (P13864), GaDNMT1: *Gallus gallus* DNMT1 (Q92072), XeDNMT1: *Xenopus laevis* DNMT1 (P79922), DrDNMT1: *Danio rerio* DNMT1 (F1RCN0), ApDNMT1A: *Apis mellifera* DNMT1A (A0A088A7M4), ArMET1: *Arabidopsis thaliana* MET1 (P34881), OsMET1B: *Oryza sativa subsp. Japonica* MET1B (B1Q3J6), DIM-2:

Neurospora crassa DIM-2 (Q3Y3Z1). The conserved threonine and tryptophan among these species are showed white characters and highlighted in black. The residues forming the hydrophobic cage are surrounded by rectangular lines and highlighted in gray. The fully conserved residues are marked asterisks. The residues of strongly and weakly similar properties are marked colons and periods, respectively. (B) Structural comparison of the TRD loops of DNMT1(291–1620)T1505A (magenta), mouse DNMT1(291–1620) (PDB accession number: 3AV4) (cyan), and human DNMT1(351–1600) (PDB accession number: 4WXX) (white). The dotted line indicates the hydrogen bond.

4.3 Comparison of the interaction manner to the essential residue in recognition of 5-methlcytosine

The crystal structures of DNMT1(731–1602) in complex with hemi-methylated DNA and DNMT1(291–1620) show that the side chain of W1512 has a hydrogen bond with the other residue, which is T1505, but the hydrophobic cage side chains (C1501, L1502, L1515, and M1535) do not have a hydrogen bond with the side chains from the other residues (Figure 1.6B; Figure 3.6A ; Figure 4.2A) (PDB accession number: 3AV4 and 4DA4). The prokaryotic DNA (cytosine-C5) methyltransferases M.HhaI and M.HaeIII, which consist of a catalytic domain alone, also show stronger binding affinity for hemi-methylated DNA, and each crystal structure in complex with hemi-methylated DNA has been determined (Reinisch *et al*., 1995; PDB accession number: 1DCT; O'Gara *et al*., 1996; PDB accession number: 5MHT). Each 5-methyl group of non-targeted strand in these complex structures forms the sole hydrophobic interaction with the side chain of E239 for M.HhaI and with the side chain of N260 for M.HaeIII, which are located on the each TRD loop (Figure 4.2B for M.HhaI; Figure 4.2C for M.HaeIII). In M.HhaI, the side chain of E239 is imposed the spatial constraints; it is hydrogen bonded to the main chains of K234 and G236. O'Gara *et al.* reported that these spatial constraints may reflect the importance of the interaction between E239 and 5-methyl group of hemi-methylated CpG. Similarly, in M.HaeIII, the side chain of N260 forms hydrogen bonds with the side chain of R225. These interactions and the hydrogen bond between T1505 and W1512 in DNMT1 have something in common. The crystal structure and biochemical data of DNMT1(291–1620)T1505A propose that the intermolecular interaction on the essential residue in recognition of 5-methylcytosine may play a role in DNA methylation activity through structural stability of the enzyme or its TRD for some DNA (cytosine-5) methyltransferases.

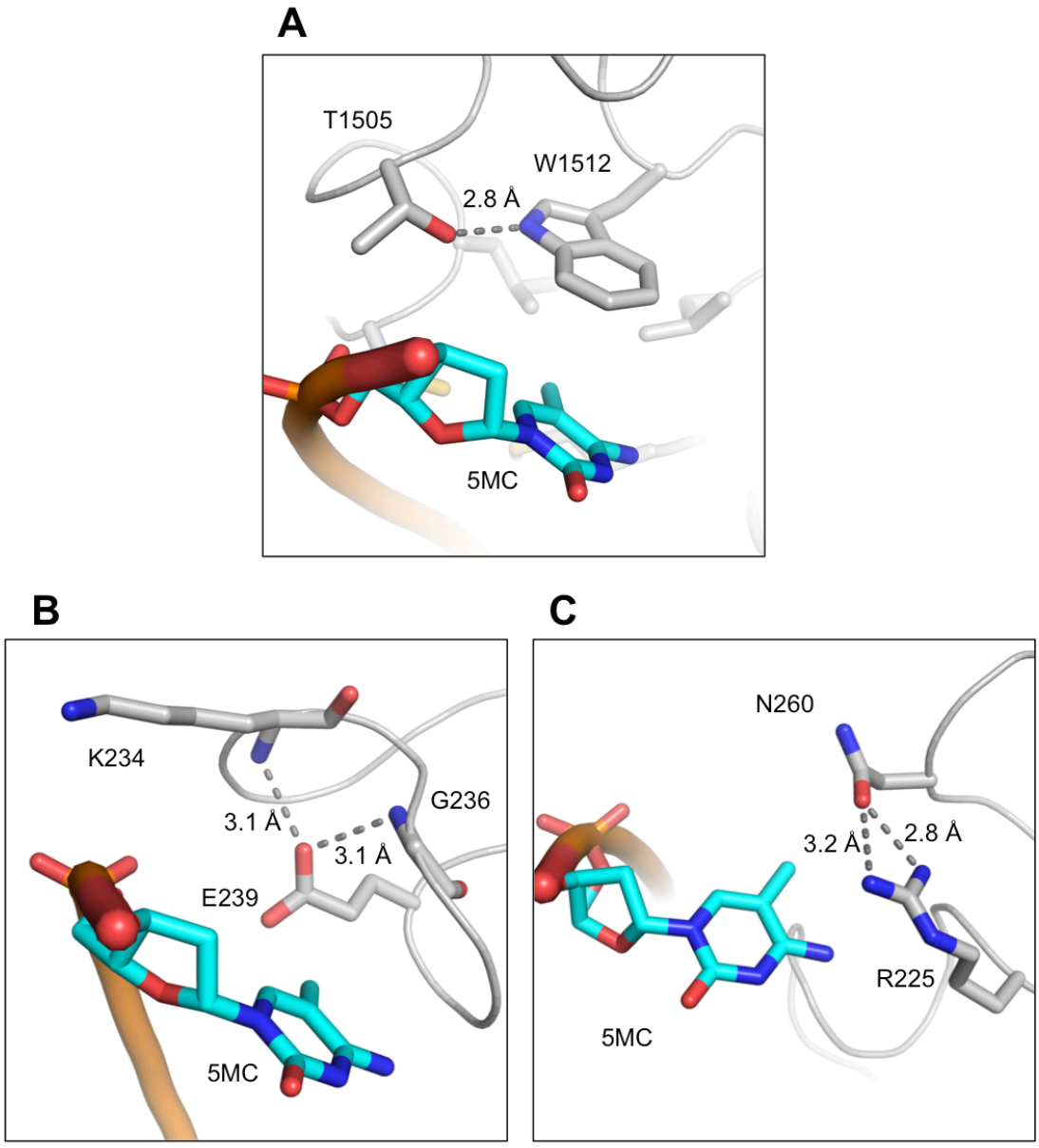

Figure 4.2 Comparison of the interaction manner to the essential residue in recognition of 5-methlcytosine.

(A) The crystal structure of mouse DNMT1(731–1602) in complex with hemi-methylated DNA (PDB accession number: 4DA4). (B) The crystal structure of M. HhaI in complex with hemi-methylated DNA (PDB accession number: 5MHT). (C) The crystal structure of M. HaeIII in complex with hemi-methylated DNA (PDB accession number: 1DCT). In all figure, dotted lines indicate the hydrogen bonds.

4.4 The trade-off between structural stability and substrate specificity of DNMT1

The specificity of DNMT1 activity for hemi-methylated DNA is achieved by the interaction between the 5-methyl group of hemi-methylated CpG and the hydrophobic cage in the TRD loop (Song *et al*., 2012); this interaction is not able to achieve during DNA methylation toward un-methylated CpG, while DNMT1(291–1620), DNMT1(602–1620), and DNMT1(731–1602) show *de novo* DNA methylation activity at about 5-fold reduction of maintenance DNA methylation activity (Takeshita *et al*., 2011; Song *et al*., 2012). Since W1512 contributes to not only forming of the hydrophobic cage but also the base-stacking interaction with the base of 5-methylcytosine (Song *et al*., 2012), DNMT1 probably possesses the base-stacking interaction between W1512 and the cytosine of un-methylated CpG during *de novo* DNA methylation. Thus, reduction in *de novo* DNA methylation activity of DNMT1(291–1620)T1505A at below 30 ºC implies that T1505A mutation could interfere with the base-stacking interaction between W1512 and the cytosine (Figure 3.8). On the other hand, since the hydrophobic cage in the TRD loop could support recognition of 5-methyl group in hemi-methylated CpG, DNMT1(291–1620)T1505A is able to possess maintenance DNA methylation activity at below 30 ºC (Figure 3.1) and consequently DNMT1(291–1620)T1505A apparently increased the specificity of maintenance DNA methylation activity (Figure 3.8C). These observations propose that the hydrogen bond between T1505 and W1512 also probably contributes to stabilizing the base-stacking interaction between W1512 and the cytosine.

De novo DNA methylation by DNMT1 *in vivo* was reported (Arand *et al*., 2012; Peters *et al*., 2013; Tajima *et al*., 2016a; Tajima *et al*., 2016b), and its activity may physiologically be meaningful. The hydrogen bond between T1505 and W1512 probably plays a role in keeping the balance between maintenance and *de novo* DNA methylation activity. DNMT1(291–1620)T1505A is superior as maintenance-type DNMT but it is

inferior from the point of view of the enzyme which functions at physiological temperature. Since DNMT1 achieves some conformation change during ongoing round of DNA methylation, the keeping of its structural stability should be a priority matter. Fundamentally, DNMT1 has to gain itself structure stability to hold stable enzymatic activity at physiological temperature. DNMT1 may have selected structural stability at the cost of higher specificity toward hemi-methylated DNA by possessing *de novo* DNA methylation activity through T1505.

Reference

Amir, R. E., Van den Veyver, I. B., Wan, M., Tran, C. Q., Francke, U., and Zoghbi, H. Y. (1999) Rett syndrome is caused by mutations in X-linked MECP2, encoding methyl-CpG-binding protein 2. *Nat. Genet.* **23**, 185–188.

Arand, J., Spieler, D., Karius, T., Branco, M. R., Meilinger, D., Meissner, A., Jenuwein, T., Xu, G., Leonhardt, H., Wolf, V., and Walter, J. (2012) In Vivo Control of CpG and Non-CpG DNA Methylation by DNA Methyltransferases. *PLoS Genet.* **8**, e1002750.

Arita, K., Ariyoshi, M., Tochio, H., Nakamura, Y., and Shirakawa, M. (2008) Recognition of hemi-methylated DNA by the SRA protein UHRF1 by a base-flipping mechanism. *Nature* **455**, 818–821.

Avvakumov, G. V, Walker, J. R., Xue, S., Li, Y., Duan, S., Bronner, C., Arrowsmith, C. H., and Dhe-Paganon, S. (2008) Structural basis for recognition of hemi-methylated DNA by the SRA domain of human UHRF1. *Nature* **455**, 822–825.

Bell, A. C., West, A. G., and Felsenfeld, G. (1999) The protein CTCF is required for the enhancer blocking activity of vertebrate insulators. *Cell* **98**, 387–396.

Bell, A. C., and Felsenfeld, G. (2000) Methylation of a CTCF-dependent boundary controls imprinted expression of the Igf2 gene. *Nature* **405**, 482–485.

Berger, S. L., Kouzarides, T., Shiekhattar, R., and Shilatifard, A. (2009) An

operational definition of epigenetics. *Genes Dev.* **23**, 781–783.

Berkyurek, A. C., Suetake, I., Arita, K., Takeshita, K., Nakagawa, A., Shirakawa, M., and Tajima, S. (2014) The DNA methyltransferase Dnmt1 directly interacts with the SET and RING finger-associated (SRA) domain of the multifunctional protein Uhrf1 to facilitate accession of the catalytic center to hemi-methylated DNA. *J. Biol. Chem.* **289**, 379–386.

Bogdanović, O., and Veenstra, G. J. (2009) DNA methylation and methyl-CpG binding proteins: Developmental requirements and function. *Chromosoma*. **118**, 549–565.

Bostick, M., Kim, J. K., Esteve, P.-O., Clark, A., Pradhan, S., and Jacobsen, S. E. (2007) UHRF1 plays a role in maintaining DNA methylation in mammalian cells. *Science* **317**, 1760–1764.

Bourc'his, D., and Bestor, T. H. (2004) Meiotic catastrophe and retrotransposon reactivation in male germ cells lacking Dnmt3L. *Nature* **431**, 96–99.

Campanero, M. R., Armstrong, M. I., and Flemington, E. K. (2000) CpG methylation as a mechanism for the regulation of E2F activity. *Proc. Natl. Acad. Sci. U. S. A.* **97**, 6481–6486.

Cheng, J., Yang, H., Fang, J., Ma, L., Gong, R., Wang, P., Li, Z., and Xu, Y. (2015) Molecular mechanism for USP7-mediated DNMT1 stabilization by acetylation. *Nat. Commun.* **6**, 7023–7033.

Cheng, X., and Blumenthal, R. M. (2010) Coordinated chromatin control: Structural and functional linkage of DNA and histone methylation. *Biochemistry*. **49**, 2999–3008.

Chuang, L. S., Ian, H. I., Koh, T. W., Ng, H. H., Xu, G. L., and Li, B. F. (1997) Human DNA (cytosine-5) methyltransferase PCNA complex as a target for p21(WAF1). *Science* **277**, 1996–2000.

Deaton, A., and Bird, A. (2011) CpG islands and the regulation of transcription. *Genes Dev.* **25**, 1010–1022.

Du, J., Johnson, L. M., Jacobsen, S. E., and Patel, D. J. (2015) DNA methylation pathways and their crosstalk with histone methylation. *Nat. Rev. Mol. Cell Biol.* **16**, 519–532.

Du, J., Zhong, X., Bernatavichute, Y. V., Stroud, H., Feng, S., Caro, E., Vashisht, A. A., Terragni, J., Chin, H. G., Tu, A., Hetzel, J., Wohlschlegel, J. A., Pradhan, S., Patel, D. J., and Jacobsen, S. E. (2012) Dual binding of chromomethylase domains to H3K9me2-containing nucleosomes directs DNA methylation in plants. *Cell* **151**, 167–180.

Ehrlich, M., Gama-Sosa, M. A., Huang, L., Midgett, R. M., Kuo, K. C., McCune, R. A., and Gehrke, C. (1982) Amount and distribution of 5-methylcytosine in human DNA from different types of tissues or cells. *Nucleic Acids Res.* **10**, 2709–2721.

Emsley, P., Lohkamp, B., Scott, W. G., and Cowtan, K. (2010) Features and

development of Coot. *Acta Crystallogr. Sect. D Biol. Crystallogr.* **66**, 486–501.

Estève, P. O., Chang, Y., Samaranayake, M., Upadhyay, A. K., Horton, J. R., Feehery, G. R., Cheng, X., and Pradhan, S. (2011) A methylation and phosphorylation switch between an adjacent lysine and serine determines human DNMT1 stability. *Nat. Struct. Mol. Biol.* **18**, 42–48.

Feng, Q., and Zhang, Y. (2001) The MeCP1 complex represses transcription through preferential binding, remodeling, and deacetylating methylated nucleosomes. *Genes Dev.* **15**, 827–832.

Filion, G. J. P., Zhenilo, S., Salozhin, S., Yamada, D., Prokhortchouk, E., and Defossez, P. A. (2006) A family of human zinc finger proteins that bind methylated DNA and repress transcription. *Mol. Cell. Biol.* **26**, 169–181.

Fu, Y., Luo, G. Z., Chen, K., Deng, X., Yu, M., Han, D., Hao, Z., Liu, J., Lu, X., Doré, L. C., Weng, X., Ji, Q., Mets, L., and He, C. (2015) N6-methyldeoxyadenosine marks active transcription start sites in Chlamydomonas. *Cell* **161**, 879–892.

Garvilles, R. G., Hasegawa, T., Kimura, H., Sharif, J., Muto, M., Koseki, H., Takahashi, S., Suetake, I., and Tajima, S. (2015) Dual functions of the RFTS domain of Dnmt1 in replication-coupled DNA methylation and in protection of the genome from aberrant methylation. *PLoS One*. **10**, 1–19.

Goll, M. G., and Bestor, T. H. (2005) Eukaryotic cytosine methyltransferases. *Annu. Rev. Biochem.* **74**, 481–514.

Goujon, M., McWilliam, H., Li, W., Valentin, F., Squizzato, S., Paern, J., and Lopez, R. (2010) A new bioinformatics analysis tools framework at EMBL-EBI. *Nucleic Acids Res.* **38**, 695–699.

Greer, E. L., Blanco, M. A., Gu, L., Sendinc, E., Liu, J., Aristizábal-Corrales, D., Hsu, C. H., Aravind, L., He, C., and Shi, Y. (2015) DNA methylation on N6-adenine in C. elegans. *Cell*. **161**, 868–878.

Guo, J. U., Su, Y., Shin, J. H., Shin, J., Li, H., Xie, B., Zhong, C., Hu, S., Le, T., Fan, G., Zhu, H., Chang, Q., Gao, Y., Ming, G., and Song, H. (2014) Distribution, recognition and regulation of non-CpG methylation in the adult mammalian brain. *Nat Neurosci*. **17**, 215–222.

Guo, X., Wang, L., Li, J., Ding, Z., Xiao, J., Yin, X., He, S., Shi, P., Dong, L., Li, G., Tian, C., Wang, J., Cong, Y., and Xu, Y. (2015) Structural insight into autoinhibition and histone H3-induced activation of DNMT3A. *Nature* **517**, 640–644.

Hark, A. T., Schoenherr, C. J., Katz, D. J., Ingram, R. S., Levorse, J. M., and Tilghman, S. M. (2000) CTCF mediates methylation-sensitive enhancer-blocking activity at the H19/Igf2 locus. *Nature* **405**, 486–489.

Hashimoto, H., Horton, J. R., Zhang, X., Bostick, M., Jacobsen, S. E., and Cheng, X. (2008) The SRA domain of UHRF1 flips 5-methylcytosine out of the DNA helix. *Nature* **455**, 826–829.

Hashimoto, H., Zhang, X., Vertino, P. M., and Cheng, X. (2015) The mechanisms of

generation, recognition, and erasure of DNA 5-methylcytosine and thymine oxidation. *J. Biol. Chem.* **290**, 20723–20733.

Holliday, R., and Pugh, J. (1975) DNA modification mechanisms and gene activity during development. *Science* **187**, 226–232.

Hotchikiss, R. D. (1948) The quantitative separation of purines, pyrimidines, and nucleosides by paper chromatography. *J. Biol. Chem.* **175**, 315–332.

Iguchi-Ariga, S. M., and Schaffner, W. (1989) CpG methylation of the cAMP-responsive enhancer / promoter sequence TGACGTCA abolishes specific factor binding as well as transcriptional activation. *Genes Dev.* **3**, 612–619.

Jia, D., Jurkowska, R. Z., Zhang, X., Jeltsch, A., and Cheng, X. (2007) Structure of Dnmt3a bound to Dnmt3L suggests a model for de novo DNA methylation. *Nature* **449**, 248–251.

Jones, P. A. (2012) Functions of DNA methylation: islands, start sites, gene bodies and beyond. *Nat. Rev. Genet.* **13**, 484–492.

Jørgensen, H. F., Ben-Porath, I., and Bird, A. P. (2004) Mbd1 is recruited to both methylated and nonmethylated CpGs via distinct DNA binding domains. *Mol. Cell. Biol.* **24**, 3387–3395.

Kameshita, I., Sekiguchi, M., Hamasaki, D., Sugiyama, Y., Hatano, N., Suetake, I., Tajima, S., and Sueyoshi, N. (2008) Cyclin-dependent kinase-like 5 binds and

phosphorylates DNA methyltransferase 1. *Biochem. Biophys. Res. Commun.* **377**, 1162–1167.

Kaneda, M., Okano, M., Hata, K., Sado, T., Tsujimoto, N., Li, E., and Sasaki, H. (2004) Essential role for de novo DNA methyltransferase Dnmt3a in paternal and maternal imprinting. *Nature* **429**, 900–903.

Kar, S., Deb, M., Sengupta, D., Shilpi, A., Parbin, S., Torrisani, J., Pradhan, S., and Patra, S. K. (2012) An insight into the various regulatory mechanisms modulating human DNA methyltransferase 1 stability and function. *Epigenetics*. **7**, 994–1007.

Kim, G. Do, Ni, J., Kelesoglu, N., Roberts, R. J., and Pradhan, S. (2002) Co-operation and communication between the human maintenance and de novo DNA (cytosine-5) methyltransferases. *EMBO J.* **21**, 4183–4195.

Kouzarides, T. (2007) Chromatin Modifications and Their Function. *Cell* **128**, 693–705.

Krissinel, E., and Henrick, K. (2004) Secondary-structure matching (SSM), a new tool for fast protein structure alignment in three dimensions. *Acta Crystallogr. Sect. D Biol. Crystallogr.* **60**, 2256–2268.

Kucharski, R., Maleszka, J., Foret, S., and Maleszka, R. (2008) Nutritional control of reproductive status in honeybees via DNA methylation. *Science* **319**, 1827–1830.

Kumar, S., Cheng, X., Klimasauskas, S., Sha, M., Posfai, J., Roberts, R. J., and

Wilson, G. G. (1994) The DNA (cytosine-5) methyltransferases. *Nucleic Acids Res.* **22**, 1–10.

Laurent, L., Wong, E., Li, G., Laurent, L., Wong, E., Li, G., Huynh, T., Tsirigos, A., Ong, C. T., Low, H. M., Wing, K., and Sung, K. (2010) Dynamic changes in the human methylome during differentiation Dynamic changes in the human methylome during differentiation. *Genome Res*. **20**, 320–331.

Law, J. A., and Jacobsen, S. E. (2010) Establishing, maintaining and modifying DNA methylation patterns in plants and animals. *Nat. Rev. Genet.* **11**, 204–220.

Leonhardt, H., Page, A. W., Weier, H. U., and Bestor, T. H. (1992) A targeting sequence directs DNA methyltransferase to sites of DNA replication in mammalian nuclei. *Cell* **71**, 865–873.

Li, E., Beard, C., and Jaenisch, R. (1993) Role for DNA methylation in genomic imprinting. *Nature* **366**, 362–365.

Li, E., and Zhang, Y. (2014) DNA Methylation in Mammals. *Cold Spring Harb. Perspect. Biol.* 10.1101/cshperspect.a019133.

Lister, R., Pelizzola, M., Dowen, R. H., Hawkins, R. D., Hon, G., Tonti-Filippini, J., Nery, J. R., Lee, L., Ye, Z., Ngo, Q.-M., Edsall, L., Antosiewicz-Bourget, J., Stewart, R., Ruotti, V., Millar, A. H., Thomson, J. a, Ren, B., and Ecker, J. R. (2009) Human DNA methylomes at base resolution show widespread epigenomic differences. *Nature* **462**, 315–322.

Long, H. K., Sims, D., Heger, A., Blackledge, N. P., Kutter, C., Wright, M. L., Grützner, F., Odom, D. T., Patient, R., Ponting, C. P., and Klose, R. J. (2013) Epigenetic conservation at gene regulatory elements revealed by non-methylated DNA profiling in seven vertebrates. *Elife*. **2013**, 1–19.

Lovell, S. C., Davis, I. W., Adrendall, W. B. III., de Bakker, P. I. W., Word, J. M., Prisant, M. G., Richardson, J. S., and Richardson, D. C. (2003) Structure validation by Calpha geometry: phi,psi and Cbeta deviation. *Proteins-Structure Funct. Genet.* **50**, 437–450.

Luger, K., Mäder, A. W., Richmond, R. K., Sargent, D. F., and Richmond, T. J. (1997) Crystal structure of the nucleosome core particle at 2.8 Å resolution. *Nature* **389**, 251–260.

Margueron, R., and Reinberg, D. (2010) Chromatin structure and the inheritance of epigenetic information. *Nat. Rev. Genet.* **11**, 285–296.

McWilliam, H., Li, W., Uludag, M., Squizzato, S., Park, Y. M., Buso, N., Cowley, A. P., and Lopez, R. (2013) Analysis Tool Web Services from the EMBL-EBI. *Nucleic Acids Res.* **41**, 597–600.

Morselli, M., Pastor, W. A., Montanini, B., Nee, K., Ferrari, R., Fu, K., Bonora, G., Rubbi, L., Clark, A. T., Ottonello, S., Jacobsen, S. E., and Pellegrini, M. (2015) In vivo targeting of de novo DNA methylation by histone modifications in yeast and mouse. *Elife*. **2015**, 1–21.

Murshudov, G. N., Vagin, A. A., and Dodson, E. J. (1997) Refinement of macromolecular structures by the maximum-likelihood method. *Acta Crystallogr. Sect. D Biol. Crystallogr.* **53**, 240–255.

Nan, X., Ng, H. H., Johnson, C. A., Laherty, C. D., Turner, B. M., Eisenman, R. N., and Bird, A. (1998) Transcriptional repression by the methyl-CpG-binding protein MeCP2 involves a histone deacetylase complex. *Nature* **393**, 386–389.

Niederhuth, C. E., and Schmitz, R. J. (2016) Putting DNA methylation in context: from genomes to gene expression in plants. *Biochim. Biophys. Acta - Gene Regul. Mech.* 10.1016/j.bbagrm.2016.08.009.

Nishiyama, A., Yamaguchi, L., Sharif, J., Johmura, Y., Kawamura, T., Nakanishi, K., Shimamura, S., Arita, K., Kodama, T., Ishikawa, F., Koseki, H., and Nakanishi, M. (2013) Uhrf1-dependent H3K23 ubiquitylation couples maintenance DNA methylation and replication. *Nature* **502**, 249–253.

Okano, M., Bell, D. W., Haber, D. A., and Li, E. (1999) DNA methyltransferases Dnmt3a and Dnmt3b are essential for de novo methylation and mammalian development. *Cell* **99**, 247–257.

Onishi, M., Liou, G. G., Buchberger, J. R., Walz, T., and Moazed, D. (2007) Role of the conserved Sir3-BAH domain in nucleosome binding and silent chromatin assembly. *Mol. Cell*. **28**, 1015–1028.

Otani, J., Nankumo, T., Arita, K., Inamoto, S., Ariyoshi, M., and Shirakawa, M.

(2009) Structural basis for recognition of H3K4 methylation status by the DNA methyltransferase 3A ATRX-DNMT3-DNMT3L domain. *EMBO Rep*. **10**, 1235–1241.

Otwinowski, Z., and Minor, W. (1997) Processing of X-ray Diffraction Data Collected in Oscillation Mode. *Methods Enzymol.* **276**, 307–326.

O'Gara, M., Roberts, R. J., and Cheng, X. (1996) A structural basis for the preferential binding of hemimethylated DNA by HhaI DNA methyltransferase. *J. Mol. Biol.* **263**, 597–606.

Peters, S. L., Hlady, R. A., Opavska, J., Klinkebiel, D., Novakova, S., Smith, L. M., Lewis, R. E., Karpf, A. R., Simpson, M. A., Wu, L., and Opavsky, R. (2013) Essential role for Dnmt1 in the prevention and maintenance of MYC-induced T-cell lymphomas. *Mol. Cell. Biol.* **33**, 4321–4333.

Pradhan, S., and Kim, G. Do (2002) The retinoblastoma gene product interacts with maintenance human DNA (cytosine-5) methyltransferase and modulates its activity. *EMBO J.* **21**, 779–788.

Qin, W., Leonhardt, H., and Pichler, G. (2011) Regulation of DNA methyltransferase 1 by interactions and modifications. *Nucleus*. **2**, 392–402.

Qin, W., Wolf, P., Liu, N., Link, S., Smets, M., Mastra, F. La, Forné, I., Pichler, G., Hörl, D., Fellinger, K., Spada, F., Bonapace, I. M., Imhof, A., Harz, H., and Leonhardt,

H. (2015) DNA methylation requires a DNMT1 ubiquitin interacting motif (UIM) and histone ubiquitination. *Cell Res.* **25**, 911–929.

Ramsahoye, B. H., Biniszkiewicz, D., Lyko, F., Clark, V., Bird, A. P., and Jaenisch, R. (2000) Non-CpG methylation is prevalent in embryonic stem cells and may be mediated by DNA methyltransferase 3a. *Proc. Natl. Acad. Sci.* **97**, 5237–5242.

Reik, W. (2007) Stability and flexibility of epigenetic gene regulation in mammalian development. *Nature* **447**, 425–432.

Reinisch, K. M., Chen, L., Verdine, G. L., and Lipscomb, W. N. (1995) The crystal structure of HaeIII methyltransferase convalently complexed to DNA: an extrahelical cytosine and rearranged base pairing. *Cell* **82**, 143–153.

Riggs, A. D. (1975) X inactivation, differentiation, and DNA methylation. *Cytogenet. Cell Genet.* **14**, 9–25.

Rondelet, G., Dal Maso, T., Willems, L., and Wouters, J. (2016) Structural basis for recognition of histone H3K36me3 nucleosome by human de novo DNA methyltransferases 3A and 3B. *J. Struct. Biol.* **194**, 357–367.

Rose, N. R., and Klose, R. J. (2014) Understanding the relationship between DNA methylation and histone lysine methylation. *Biochim. Biophys. Acta - Gene Regul. Mech.* **1839**, 1362–1372.

Rountree, M. R., Bachman, K. E., and Baylin, S. B. (2000) DNMT1 binds HDAC2

and a new co-repressor, DMAP1, to form a complex at replication foci. *Nat. Genet.* **25**, 269–277.

Ruthenburg, A. J., Li, H., Patel, D. J., and Allis, C. D. (2007) Multivalent engagement of chromatin modifications by linked binding modules. *Nat. Rev. Mol. Cell Biol.* **8**, 983–994.

Sakai, Y., Suetake, I., Shinozaki, F., Yamashina, S., and Tajima, S. (2004) Co-expression of de novo DNA methyltransferases Dnmt3a2 and Dnmt3L in gonocytes of mouse embryos. *Gene Expr. Patterns*. **5**, 231–237.

Sarraf, S. A., and Stancheva, I. (2004) Methyl-CpG binding protein MBD1 couples histone H3 methylation at lysine 9 by SETDB1 to DNA replication and chromatin assembly. *Mol. Cell*. **15**, 595–605.

Sharif, J., Muto, M., Takebayashi, S., Suetake, I., Iwamatsu, A., Endo, T. A., Shinga, J., Mizutani-Koseki, Y., Toyoda, T., Okamura, K., Tajima, S., Mitsuya, K., Okano, M., and Koseki, H. (2007) The SRA protein Np95 mediates epigenetic inheritance by recruiting Dnmt1 to methylated DNA. *Nature* **450**, 908–912.

Shirane, K., Toh, H., Kobayashi, H., Miura, F., Chiba, H., Ito, T., Kono, T., and Sasaki, H. (2013) Mouse Oocyte Methylomes at Base Resolution Reveal Genome-Wide Accumulation of Non-CpG Methylation and Role of DNA Methyltransferases. *PLoS Genet.* 10.1371/journal.pgen.1003439.

Sievers, F., Wilm, A., Dineen, D., Gibson, T. J., Karplus, K., Li, W., Lopez, R.,

McWilliam, H., Remmert, M., Söding, J., Thompson, J. D., and Higgins, D. G. (2011) Fast, scalable generation of high-quality protein multiple sequence alignments using Clustal Omega. *Mol. Syst. Biol.* **7**, 539.

Song, J., Rechkoblit, O., Bestor, T. H., and Patel, D. J. (2011) Structure of DNMT1-DNA complex reveals a role for autoinhibition in maintenance DNA methylation. *Science* **331**, 1036–1040.

Song, J., Teplova, M., Ishibe-Murakami, S., and Patel, D. J. (2012) Structure-based mechanistic insights into DNMT1-mediated maintenance DNA methylation. *Science*. **335**, 709–712.

Suetake, I., Hayata, D., and Tajima, S. (2006) The amino-terminus of mouse DNA methyltransferase 1 forms an independent domain and binds to DNA with the sequence involving PCNA binding motif. *J. Biochem.* **140**, 763–776.

Suetake, I., Miyazaki, J., Murakami, C., Takeshima, H., and Tajima, S. (2003) Distinct enzymatic properties of recombinant mouse DNA methyltransferases Dnmt3a and Dnmt3b. *J. Biochem.* **133**, 737–744.

Suetake, I., Shinozaki, F., Miyagawa, J., Takeshima, H., and Tajima, S. (2004) DNMT3L stimulates the DNA methylation activity of Dnmt3a and Dnmt3b through a direct interaction. *J. Biol. Chem.* **279**, 27816–27823.

Sugiyama, Y., Hatano, N., Sueyoshi, N., Suetake, I., Tajima, S., Kinoshita, E., Kinoshita-Kikuta, E., Koike, T., and Kameshita, I. (2010) The DNA-binding activity

of mouse DNA methyltransferase 1 is regulated by phosphorylation with casein kinase 1delta/epsilon. *Biochem. J.* **427**, 489–497.

Syeda, F., Fagan, R. L., Wean, M., Avvakumov, G. V., Walker, J. R., Xue, S., Dhe-Paganon, S., and Brenner, C. (2011) The replication focus targeting sequence (RFTS) domain is a DNA-competitive inhibitor of Dnmt1. *J. Biol. Chem.* **286**, 15344–15351.

Tajima, S., Kimura, H., and Suetake, I. (2016a) Establishment and Maintenance of DNA Methylation. in *DNA Replication, Recombination, and Repair* (Hanaoka, F., and Sugasawa, K. eds), pp. 489–516, Springer Japan, Tokyo, 10.1007/978-4-431-55873-6_20.

Tajima, S., Suetake, I., Takeshita, K., Nakagawa, A., and Kimura, H. (2016b) Domain Structure of the Dnmt1, Dnmt3a, and Dnmt3b DNA Methyltransferases. in *DNA Methyltransferases - Role and Function* (Jeltsch, A., and Jurkowska, R. Z. eds), pp. 63–86, Springer International Publishing, Cham, 10.1007/978-3-319-43624-1_4.

Takeshita, K., Suetake, I., Yamashita, E., Suga, M., Narita, H., Nakagawa, A., and Tajima, S. (2011) Structural insight into maintenance methylation by mouse DNA methyltransferase 1 (Dnmt1). *Proc. Natl. Acad. Sci. U. S. A.* **108**, 9055–9059.

Tamaru, H., and Selker, E. U. (2001) A histone H3 methyltransferase controls DNA methylation in Neurospora crassa. *Nature* **414**, 277–283.

Ushijima, T., Watanabe, N., Okochi, E., Kaneda, A., Sugimura, T., and Miyamoto, K. (2003) Fidelity of the methylation pattern and its variation in the genome. *Genome*

Res. **13**, 868–874.

Vagin, A., and Teplyakov, A. (2010) Molecular replacement with MOLREP. *Acta Crystallogr. Sect. D Biol. Crystallogr.* **66**, 22–25.

Vilkaitis, G., Suetake, I., Klimasauskas, S., and Tajima, S. (2005) Processive methylation of hemimethylated CpG sites by mouse Dnmt1 DNA methyltransferase. *J. Biol. Chem.* **280**, 64–72.

Walsh, C., Chaillet, J., and Bestor, T. (1998) Transcription of IAP endogenous retroviruses is constrained by cytosine methylation. *Nat. Genet.* **20**, 116–117.

Wang, Y., Jorda, M., Jones, P. L., Maleszka, R., Ling, X., Robertson, H. M., Mizzen, C. A., Peinado, M. A., and Robinson, G. E. (2006) Functional CpG methylation system in a social insect. *Science* **314**, 645–647.

Watanabe, D., Suetake, I., Tada, T., and Tajima, S. (2002) Stage- and cell-specific expression of Dnmt3a and Dnmt3b during embryogenesis. *Mech. Dev.* **118**, 187–190.

Wilson, G. G., and Murray, N. E. (1991) Restriction and Modification. *Annu. Rev. Genet.* **25**, 585–627.

Winkelmann, J., Lin, L., Schormair, B., Kornum, B. R., Faraco, J., Plazzi, G., Melberg, A., Cornelio, F., Urban, A. E., Pizza, F., Poli, F., Grubert, F., Wieland, T., Graf, E., Hallmayer, J., Strom, T. M., and Mignot, E. (2012) Mutations in DNMT1 cause autosomal dominant cerebellar ataxia, deafness and narcolepsy. *Hum. Mol.*

Genet. **21**, 2205–2210.

Winn, M. D., Ballard, C. C., Cowtan, K. D., Dodson, E. J., Emsley, P., Evans, P. R., Keegan, R. M., Krissinel, E. B., Leslie, A. G. W., McCoy, A., McNicholas, S. J., Murshudov, G. N., Pannu, N. S., Potterton, E. A., Powell, H. R., Read, R. J., Vagin, A., and Wilson, K. S. (2011) Overview of the CCP4 suite and current developments. *Acta Crystallogr. Sect. D Biol. Crystallogr.* **67**, 235–242.

Wu, J. C., and Santi, D. V. (1987) Kinetic and catalytic mechanism of HhaI methyltransferase. *J. Biol. Chem.* **262**, 4778–4786.

Yamauchi, T., Johzuka-Hisatomi, Y., Terada, R., Nakamura, I., and Iida, S. (2014) The MET1b gene encoding a maintenance DNA methyltransferase is indispensable for normal development in rice. *Plant Mol. Biol.* **85**, 219–232.

Yang, J., Lior-Hoffmann, L., Wang, S., Zhang, Y., and Broyde, S. (2013) DNA cytosine methylation: Structural and thermodynamic characterization of the epigenetic marking mechanism. *Biochemistry*. **52**, 2828–2838.

Yoon, H. G., Chan, D. W., Reynolds, A. B., Qin, J., and Wong, J. (2003) N-CoR mediates DNA methylation-dependent repression through a methyl CpG binding protein Kaiso. *Mol. Cell*. **12**, 723–734.

Zhang, G., Huang, H., Liu, D., Cheng, Y., Liu, X., Zhang, W., Yin, R., Zhang, D., Zhang, P., Liu, J., Li, C., Liu, B., Luo, Y., Zhu, Y., Zhang, N., He, S., He, C., Wang, H., and Chen, D. (2015) N6-methyladenine DNA modification in Drosophila. *Cell*

161, 893–906.

Zhang, Z. M., Liu, S., Lin, K., Luo, Y., Perry, J. J., Wang, Y., and Song, J. (2015) Crystal structure of human DNA methyltransferase 1. *J. Mol. Biol.* **427**, 2520–2531.

List of publication

Kanada, K., Takeshita, K., Suetake, I., Tajima, S., and Nakagawa, A. (2017) Conserved threonine 1505 in the catalytic domain stabilizes mouse DNMT1. *J. Biochem*. Epub ahead of print.